JGR Biogeosciences

RESEARCH ARTICLE
10.1029/2024JG008537

Assessing the Molecular-Level Controls of Dissolved Organic Matter Cycling in West Siberian Lowland Rivers

Martin R. Kurek[1,2], Oleg S. Pokrovsky[3], Ivan V. Krickov[4], Artem G. Lim[4], Mikhail A. Korets[5], and Robert G. M. Spencer[1,2]

[1]Department of Earth, Ocean and Atmospheric Science, Florida State University, Tallahassee, FL, USA, [2]National High Magnetic Field Laboratory Geochemistry Group, Tallahassee, FL, USA, [3]Geosciences and Environment Toulouse, UMR 5563 CNRS, University of Toulouse, Toulouse, France, [4]BIO-GEO-CLIM Laboratory, Tomsk State University, Tomsk, Russia, [5]V.N. Sukachev Institute of Forest, Siberian Branch of Russian Academy of Sciences, Krasnoyarsk, Russia

Key Points:

- Seasonality controls dissolved organic matter (DOM) composition and concentration in West Siberian Lowland rivers
- Molecular signatures indicate shifting DOM sources between surface litter and subsurface soil from spring flood to summer flow
- Peatland, needleleaf forest, and broadleaf forest cover are important secondary controls of West Siberian Lowland river DOM composition

Supporting Information:

Supporting Information may be found in the online version of this article.

Correspondence to:

M. R. Kurek,
mkurek@fsu.edu

Citation:

Kurek, M. R., Pokrovsky, O. S., Krickov, I. V., Lim, A. G., Korets, M. A., & Spencer, R. G. M. (2025). Assessing the molecular-level controls of dissolved organic matter cycling in West Siberian Lowland rivers. *Journal of Geophysical Research: Biogeosciences*, *130*, e2024JG008537. https://doi.org/10.1029/2024JG008537

Received 8 OCT 2024
Accepted 11 MAR 2025

Abstract The West Siberian Lowland (WSL) contains some of the largest wetlands and most extensive peatlands on Earth, storing vast amounts of vulnerable carbon across permafrost-free to continuous permafrost zones. As temperature and precipitation changes continue to alter the Siberian landscape, carbon transfer to the atmosphere and export to the Arctic Ocean will be impacted. However, the drivers of organic carbon transfer are largely unknown across this region. We characterized seasonal dissolved organic carbon (DOC) concentration and dissolved organic matter (DOM) composition of WSL rivers from the middle reaches of the Ob' River in the permafrost-free zone, as well as tributaries of the Taz River in the northern continuous permafrost zone. DOC and aromatic DOM properties increased from spring to autumn in the Ob' tributaries, reflecting the seasonal transition from groundwater-sourced to terrestrial DOM. Differences in molecular-level signatures via ultra-high resolution mass spectrometry revealed the influence of redox processes on DOM composition in the winter while terrestrial DOM sourcing shifted from surface litter aliphatics and highly unsaturated and phenolic high-O/C ($HUP_{High\ O/C}$) compounds in the spring to subsurface soils and $HUP_{Low\ O/C}$ compounds by autumn. Furthermore, aromaticity and organic N were related to landscape properties including peatlands, forest cover, and the ratio of needleleaf:broadleaf forests. Finally, the Taz River tributaries were similar to summer and autumn Ob' tributaries, but more enriched in N and S-containing compounds. These signatures were likely derived from thawing permafrost, which we expect to increase in northern rivers due to active layer expansion in a warming Arctic.

Plain Language Summary Dissolved organic matter (DOM) is central to atmospheric greenhouse gas transfer and land-ocean carbon export from rivers, particularly in northern arctic regions that are warming faster than the global average. However, seasonal effects of DOM cycling in rivers remain understudied across these regions, such as in the West Siberian Lowland (WSL) which store a vast amount of carbon in some of the largest wetlands and peatlands on Earth. We characterized DOM in permafrost-free rivers from the WSL from winter to early autumn and compared their characteristics to northern rivers in the continuous permafrost zone. Seasonality was the primary factor explaining differences in DOM sourcing and processing across the rivers. Riverine DOM was dominated by groundwater inputs during winter, surface layers and vegetation in the spring, and deeper subsurface soil by autumn. Finally, landscape properties accounted for additional differences in DOM composition between the rivers. Northern rivers contained permafrost-derived signatures that were absent in the southern WSL, while peatland and forest coverage influenced organic N content. Landscape disturbances including permafrost thaw will likely mobilize more biologically labile DOM signatures into rivers which will impact the balance between greenhouse gas emissions and lateral carbon export from this region.

1. Introduction

High-latitude arctic systems represent a massive global carbon sink with 1,460–1,600 Pg C stored in permafrost soils and an additional 250–450 Pg C in northern peatlands (Gorham, 1991; Hugelius et al., 2014, 2020; Limpens et al., 2008; Schuur et al., 2015, 2022; Tarnocai et al., 2009). These regions contribute disproportionately to global carbon cycling via atmospheric greenhouse gas emissions (Karlsson et al., 2021; Schuur et al., 2015) and lateral carbon transfer to aquatic systems as driven by anthropogenic climate change (Gandois et al., 2021; Holmes et al., 2012; Raymond et al., 2007; Starr et al., 2023). High-latitude arctic systems are warming 2–3 times faster than the global average (Davy & Outten, 2020; Schuur et al., 2022) leading to active layer thaw and a northward

migration of the permafrost boundary. Such changes have released ancient permafrost carbon, nutrients, and altered subsurface flow paths (Frey & McClelland, 2009; Frey et al., 2007; Miner et al., 2022; Plaza et al., 2019; Romanovsky et al., 2010; Schuur et al., 2015). Warming has also led to longer growing seasons and vegetation expansion in the northern tundra known as "greening" (Berner et al., 2020; Forbes et al., 2010; Miles & Esau, 2016), which may also impact organic carbon delivery and atmospheric cycling in connected waterways (Catalán et al., 2024). Furthermore, these landscapes are also impacted by changing precipitation patterns, including more frequent extreme events (Sada et al., 2019; Xu et al., 2020), and anthropogenic disturbances such as wildfires, deforestation, and resource extraction (Ivanov et al., 2022; Kirpotin et al., 2021; Kühling et al., 2016). Such disturbances have mobilized aged carbon and nutrients from the landscape and modified the chemical signatures of exported organic carbon across other connected aquatic systems (Drake et al., 2019; Drake, Guillemette, et al., 2018; Rodríguez-Cardona et al., 2020; Wilson & Xenopoulos, 2009). Together, climatic and anthropogenic changes will likely impact ecosystem and carbon balance in rivers across these regions (e.g., Karlsson et al., 2021; Krickov et al., 2021; Serikova et al., 2018, 2019), making it important to understand the sourcing and contribution of different carbon pools to CO_2 outgassing and overall export.

Dissolved organic carbon (DOC) is an essential component of the carbon cycle, representing the quantified portion of dissolved organic matter (DOM) and serving as an important link between terrestrial and atmospheric systems (Battin et al., 2009; Cole et al., 2007; Drake, Raymond, & Spencer, 2018; Tranvik et al., 2009). DOM represents a complex mixture of organic compounds from terrestrial and internally produced (autochthonous) sources that have undergone mixing, processing, and degradation (Berggren et al., 2022; Kellerman et al., 2018; Yvin et al., 2024). DOM serves many ecosystem functions, most notably as a carbon substrate for heterotrophic respiration and a nutrient source (Battin et al., 2009; D'Andrilli et al., 2019; Hensgens et al., 2021; Hutchins et al., 2017; Kaiser, Canedo-Oropeza, et al., 2017; Textor et al., 2019). Investigating the chemical characteristics of DOM often reveals its source and processing history, which can be used to predict how it will function in aquatic systems. For instance, DOM originating from soils or vegetation is highly aromatic and susceptible to photodegradation, but more resistant to biological degradation on short timescales. In contrast, DOM from algal or microbial sources is more aliphatic and rapidly consumed by microorganisms, and considered to be photostable (Begum et al., 2023; Berggren et al., 2022; Cory et al., 2015; Guillemette et al., 2013; Koehler et al., 2012; Textor et al., 2019). Highly aromatic chromophoric DOM (CDOM) is also important for surface heat transfer and influences primary productivity, especially in coastal and marine waters (Hancke et al., 2012; Hill, 2008; Osburn et al., 2009). However, DOM from fresh vegetation and thawed permafrost also contain components that are biolabile whereas aged microbial DOM that has undergone extensive processing tends to be more biostable (Catalán et al., 2016; Drake, Guillemette, et al., 2018; Hensgens et al., 2021; Lapierre & Del Giorgio, 2014; Lechtenfeld et al., 2014; Spencer et al., 2015). Such contradictions highlight the importance of considering both intrinsic and extrinsic constraints when upscaling to the ecosystem level, such as across large river systems.

The West Siberian Lowland (WSL) is the world's second largest wetland complex (600,000 km^2), next to the Amazon várzea, and contains one of the largest peatlands on Earth (Frey & Smith, 2005; Kremenetski et al., 2003; Pokrovsky et al., 2015). These peatlands span permafrost-free to continuous permafrost zones and store around 70 pg C in thick deposits (Kremenetski et al., 2003; Sheng et al., 2004) which are transported into connected rivers as organic carbon (Frey & Smith, 2005; Olefeldt et al., 2013; Rosset et al., 2022). As the largest river draining the WSL and the third largest in the Arctic by discharge, the Ob' River exports about 4.12 Tg DOC into the Arctic Ocean every year (Holmes et al., 2012) where it is mixed with coastal arctic waters, and mineralized on various timescales (Drozdova et al., 2021; Hansell et al., 2004; Kaiser, Benner, & Amon, 2017; Opsahl et al., 1999). However, this delivery is contingent on seasonal patterns. Winter baseflow is low due to reduced discharge from ice cover, delivering aliphatic and aged DOM sourced from groundwater, whereas the spring delivers fresh terrestrial CDOM representing over 30% of the yearly DOC input in just under 2 months (Amon et al., 2012; Behnke et al., 2021; Gandois et al., 2021; Holmes et al., 2012; Raymond et al., 2007).

Similarly, landscape properties including peatlands, vegetation, and permafrost coverage influence DOM sourcing and processing across the WSL. The southern permafrost-free catchments supply the Ob' River with highly aromatic soil-derived DOM via connected tributaries, particularly during high discharge (Mann et al., 2016; Perminova et al., 2019; Pipko et al., 2023; Starr et al., 2024; Vorobyev et al., 2015), while northern regions drain permafrost zones that export aged and biolabile DOM to headwaters during the summer at the time of maximum active layer expansion (Krickov et al., 2024; Rogers et al., 2021; Spencer et al., 2015; Vorobyev et al., 2022). As permafrost landscapes thaw, peatlands exert greater influence over DOC export and DOM

composition into connected tributaries during inundation (Frey & Smith, 2005; Starr et al., 2023). These peatlands integrate DOM from the landscape and enhance mineralization in headwaters of the floodplain (Krickov et al., 2021; Payandi-Rolland et al., 2020; Raudina et al., 2022), while more stable DOM is exported downstream (Rosset et al., 2022). Given the significant CO_2 emissions from the WSL (Karlsson et al., 2021; Serikova et al., 2018, 2019), understanding the sourcing and seasonality of DOM from WSL rivers will become increasingly important in the face of changing permafrost boundaries, active layer thickness, and hydrology (Frey & McClelland, 2009; Miner et al., 2022; Xu et al., 2020).

While the WSL have been the subject of previous studies describing spatial relationships between DOM composition (Frey & Smith, 2005; Perminova et al., 2019; Starr et al., 2024), they have all focused on late summer flow, missing the critical impact of the spring freshet period. These studies have primarily addressed the influence of peatland and permafrost extent on carbon export but not considered the impacts of other land use types such as forest or mixed landscapes on aquatic DOM sourcing in surrounding rivers. Conversely, other studies have described both the seasonal and spatial dynamics of WSL rivers with respect to elemental geochemistry, trace metals, DOC (Krickov et al., 2020; Pokrovsky et al., 2015, 2016, 2020; Pokrovsky, Manasypov, et al., 2022; Vorobyev et al., 2019), and greenhouse gas emissions (Karlsson et al., 2021; Krickov et al., 2023, 2024; Serikova et al., 2018; Vorobyev et al., 2022), but have not incorporated them with DOM signatures. This study aims to integrate both seasonal and spatial controls in WSL rivers by investigating changes in DOC, CDOM, and molecular-level DOM composition via 21 T Fourier transform-ion cyclotron resonance mass spectrometry (FT-ICR MS), which can resolve mass differences between molecular formulae that are <1 mDa apart (Hendrickson et al., 2015; Smith et al., 2018).

The goals of this study were to: (a) describe the seasonal dynamics of DOC and DOM composition across a subset of tributaries from the middle reaches of the Ob' River from winter to early autumn, (b) investigate the drivers of molecular-level signatures across seasons, between tributaries from the middle reaches of the Ob' River, and several northern permafrost-fed tributaries during the time of maximum permafrost thaw, and (c) describe the potential impacts of catchment properties on WSL river DOM composition and organic carbon sourcing. By examining the seasonal and spatial composition of WSL river DOM, we aim to better understand large scale drivers of carbon cycling in high-latitude arctic rivers and how they may be impacted by future changes in climate and land-use.

2. Materials and Methods

2.1. Study Sites and Field Sampling

The Ob' River is the largest arctic river by watershed area (2,990,000 km^2) and supplies 15% of the total freshwater discharge to the Arctic Ocean via the Kara Sea. The middle reaches of the Ob' River (MRO) are part of the WSL and characterized by extensive flooding beginning in the spring and persisting through summer resulting in inundated floodplains, winding channels, and interconnected water bodies, described as the "flood zone" (Vorobyev et al., 2015). This study focused on rivers from the boreal taiga biome in the permafrost-free zone (Figure 1, pink points) with lithology consisting of clays, sands, and silts from alluvial, lake-alluvial, and some aeolian origin (Pokrovsky et al., 2015). Landcover is characterized by forests (broadleaf, mixed, light needleleaf, dark needleleaf), peatlands and bogs, grasslands, as well as lesser contributions from cropland and riparian vegetation (Figure S1a in Supporting Information S1). Details regarding landcover data are provided in Text S1 in Supporting Information S1. Mean annual air temperature is −0.2°C and mean annual precipitation is 502 mm yr^{-1} (Table S1 in Supporting Information S1). Eight rivers from the WSL within the middle reaches of the Ob' River (Ob' mainstem, Chaya, Parabel, Vasyugan, Chigas, Chemondaevka, Tatosh, Brovka; Table S1 in Supporting Information S1; Figure 1) were sampled in 9–10 March, 4–6 May, 8–9 June, and 9–10 September 2023 and are hereafter referred to as "MRO rivers." The Chigas River was not sampled in March and the Parabel was not sampled in September.

The lower Taz River basin is located in the tundra and forest-tundra biome within the continuous permafrost zone (Figure 1, white points). The dominant lithology of this area consists of clays, silts, and sands that are overlain by quaternary deposits (loeses, fluvial, glacial, lacustrine; Pokrovsky, Lim, et al., 2022; Pokrovsky, Manasypov, et al., 2022). Landcover is characterized by peatlands and bogs, shrub and tundra, and grassy tundra (Figure S1b in Supporting Information S1). Mean annual air temperature is −6.5°C and mean annual precipitation is 500 mm yr^{-1} (Table S1 in Supporting Information S1). Five Taz River tributaries ("Taz tributaries,"

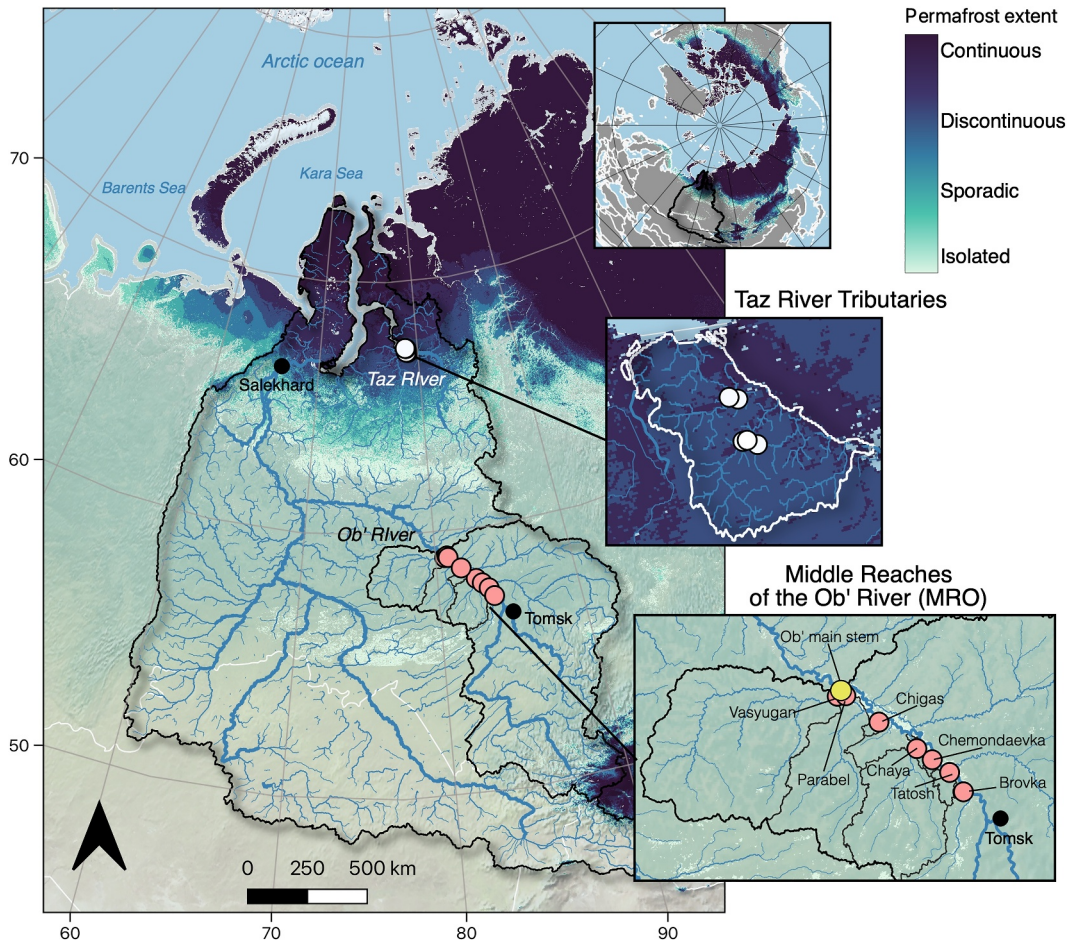

Figure 1. Map of the Ob' River watershed and sampling sites of the West Siberian Lowland (WSL) rivers. Samples were collected from tributaries in the middle reaches of the Ob' River (MRO, pink points), the Ob' River mainstem (yellow point), and small tributaries of the Taz River (white points). Watersheds of the middle and upper reaches of the Ob' River are outlined in black while the watershed of the lower Taz River is outlined in white. Permafrost extent from isolated to continuous coverage is colored from teal to blue. Reference sites for Tomsk and Salekhard are mapped as black points. Detailed landcover maps of the river basins are provided in Figure S1 in Supporting Information S1.

Sambotoyaha, Nuny Yaha, Nuny Yaha tributary, Vysakoyakha, Vysakoyakha tributary; Table S1 in Supporting Information S1; Figure 1) were sampled on 26 August 2021 and included in this study to assess differences between landcover inputs from permafrost-free rivers and continuous permafrost rivers at the time of maximum permafrost thaw.

2.2. Sample Collection and Water Quality Measurements

We collected surface water from the middle of the river at 20–30 cm depth for determination of hydrochemical parameters. In winter, the surface waters were sampled from a large (60 × 60 cm) pit in the center of the ice cover. Dissolved oxygen, pH, specific conductivity (SpC), and water temperature were measured in situ at 20 cm depth using a WTW 3320 Multimeter. The river water was sampled in pre-cleaned polypropylene bottles and immediately filtered through pyrolyzed GF/F filters using pre-cleaned Nalgene 250-mL filtration units and a manual Mityvac vacuum pump. The filtrates were acidified with ultra-pure bi-distilled HCl (2%) and immediately frozen at −18°C in the field freezer. Another portion of river water was filtered through disposable sterile Sartorius filter units (0.45 μm pore size) and acidified with 2% ultrapure bi-distilled HNO_3 for trace metal analysis. In both cases, the first 50 mL of filtrate was discarded.

2.3. DOC, DIC, and Optical Analysis

DOC (acidified) and dissolved inorganic carbon (DIC) concentrations were determined using a Shimadzu TOC-VSCN Analyzer (Kyoto, Japan) with an uncertainty of 3% and a detection limit of 0.1 mg L^{-1} using established methodology (e.g., Pokrovsky et al., 2020; Vorobyev et al., 2022). Milli-Q water blanks were passed through the filters and demonstrated negligible release of DOC from the filter material.

CDOM was quantified via UV-visible absorbance spectra measured at room temperature in a 1 cm quartz cuvette with a Horiba Scientific Aqualog (Horiba Ltd., Kyoto, Japan) at wavelengths of 230–800 nm. CDOM was determined as the Napierian absorption coefficient at 350 nm (a_{350}; m^{-1}) and at 254 nm (a_{254}; m^{-1}). Spectral slopes from absorption spectra are correlated with aromaticity and molecular weight and were calculated from 275 to 295 ($S_{275\text{-}295}$; nm^{-1}; Helms et al., 2008). Specific UV absorption at 254 nm ($SUVA_{254}$; L mg C^{-1} m^{-1}) is associated with aromatic composition and was calculated by dividing the decadic absorption coefficient at 254 nm by the DOC concentration (mg L^{-1}; Weishaar et al., 2003). For comparison, Ob' River DOC concentrations and absorption spectra from 2009 to 2021 were obtained from the Arctic Great Rivers Observatory repository (Arctic GRO; https://arcticgreatrivers.org). Finally, the fluorescence index (FI), which has been related to terrestrial and microbial contributions to DOM, was calculated from the emission intensity at 470 and 520 nm at excitation 370 nm using excitation-emission matrices also collected with the same instrument (Cory & McKnight, 2005; McKnight et al., 2001) using established protocols (e.g., Kurek et al., 2024).

2.4. Solid Phase Extraction (SPE) and FT-ICR MS Analysis

Filtered water samples were acidified (HCl, pH 2) and extracted with Bond-Elut PPL columns (Agilent Technologies Inc., Santa Clara, CA) following established procedures (Dittmar et al., 2008). Columns were conditioned by soaking with methanol overnight followed by a methanol rinse and two rinses with acidified Milli-Q water (HCl, pH 2). Approximately 50 μg C was isolated onto 100 mg 3 mL bed volume PPL columns (assuming at least 50% recovery), eluted with 1 mL methanol into precombusted (550°C, >4 hr) glass vials, and stored at −20°C until analysis. DOC recovery was assessed on several river samples with duplicate extractions. Methanol extracts were collected in 40 mL glass vials and the methanol was evaporated by gently drying (50°C, overnight). The organic residue was redissolved in Milli-Q water (HCl, pH 2) and DOC concentrations were measured using methods outlined in Section 2.3 (e.g., Kurek et al., 2024).

Methanolic extracts were analyzed on a custom-built hybrid linear ion trap ultra-high resolution FT-ICR mass spectrometer equipped with a 21T superconducting solenoid magnet at the National High Magnetic Field Laboratory (Tallahassee, FL; Hendrickson et al., 2015; Smith et al., 2018). Negatively charged ions from DOM were produced via electrospray ionization (ESI) at a flow rate of 500 nL min^{-1} via a syringe pump. Typical conditions for ion formation included: emitter voltage: −2.8–3.2 kV; S-lens RF level: 40%; and heated metal capillary temperature: 350°C. The resulting spectra were conditionally co-added to yield 100 individual time domain transients of 3.1 s each for each experiment. Co-added mass spectra were phase-corrected (Xian et al., 2010) and peaks were internally calibrated based on 10–15 highly abundant O-containing series using a "walking" calibration (Savory et al., 2011) as described previously (e.g., Kurek et al., 2024). Further details regarding FT-ICR MS methodology are provided in the supplemental methods (Text S1 in Supporting Information S1).

2.5. FT-ICR MS Post-Processing

Mass spectral peaks (>6σ root-mean-square (RMS) baseline noise) were exported to a peak list and processed using PetroOrg© (Corilo, 2014). Molecular formulae were assigned to ions constrained by $C_{4\text{-}75}H_{4\text{-}150}O_{1\text{-}30}N_{0\text{-}4}S_{0\text{-}2}$ not exceeding 300 ppb error (e.g., Kurek et al., 2024). For all spectra, between 13,000 and 22,000 species were assigned elemental compositions (mean: 17,000) with RMS error between 50 and 80 ppb (mean: 70) and achieved resolving power >1,600,000 at m/z 400. Molecular formula properties, including the modified aromaticity index (AI_{mod}) and nominal carbon oxidation state (NOSC), were calculated according to Koch and Dittmar (2006, 2016) and Boye et al. (2017), respectively. Mass-weighted stoichiometric ratios were averaged (H/C, O/C, N/C, S/C) and formulae were also grouped based on the percent relative abundance of their heteroatom classes (CHO, CHON, CHOS, and CHONS). Formulae were classified based on Šantl-Temkiv et al. (2013) which represent mixtures of broad compound classes that relate to bulk molecular properties and biolability (e.g., Hensgens et al., 2021; Kellerman et al., 2018; Kurek et al., 2023). Groups include condensed aromatic-like (CA; 0.67 < AI_{mod}), polyphenolic-like (PPh; 0.50 < AI_{mod} < 0.67), highly unsaturated and phenolic low O/C ($HUP_{Low\ O/C}$;

$AI_{mod} < 0.50$, H/C < 1.5, O/C < 0.5), highly unsaturated and phenolic high O/C ($HUP_{High\ O/C}$; $AI_{mod} < 0.50$, H/C < 1.5, $0.5 \leq$ O/C), and aliphatic-like (Ali; $1.5 \leq$ H/C), and the percent relative abundance of each class was summed. Data derived from individual mass spectra including, number of peak assignments, RMS error, and calculated properties for all species identified by 21T FT-ICR MS used in this publication are provided in Data Set S1 (Kurek, 2024).

Molecular formulae belonging to the island of stability (IOS), a group of 361 individual molecular formulae reported by Lechtenfeld et al. (2014) in marine DOM and ubiquitous in freshwaters (e.g., Behnke et al., 2021; Kellerman et al., 2018; Starr et al., 2023), were identified in each individual mass spectrum. Their relative abundances were summed to estimate the contribution of stable, aged DOM likely representing thousands of isomers from convergent degradation pathways (Kellerman et al., 2018). Similarly, we identified molecular formulae as part of the Core Arctic Riverine Fingerprint (CARF), which is a group of 1,328 individual formulae identified in the six largest arctic rivers across various years and hydroperiods (Behnke et al., 2021). The relative abundance of CARF formulae was also summed to estimate stable DOM exported to marine systems from the landscape (Kurek et al., 2024).

2.6. Geochemical Analysis

Filtered solutions for major and trace element analyses were acidified (2% ultrapure HNO_3) and were stored in pre-washed HDPE bottles. The preparation of bottles for sample storage was performed in a clean bench room (ISO A 10,000). Blanks were performed to control the level of pollution induced by sampling and filtration. Major cations (Ca, Mg, Na and K), Si, P, Al, Fe, and Mn were determined with an Agilent iCap Triple Quadrupole (TQ) ICP MS using both Ar and He modes to diminish interferences, with In and Re as internal standards added on-line, and 3 external in-house standards. These were placed each in 10 samples per series of river water. Typical analytical uncertainty was 2%. For all trace metals analyzed by ICP MS, the concentrations in blanks were below analytical detection limits. The SLRS-6 (Riverine Water Reference Material for Trace Metals certified by the National Research Council of Canada) was used to check the accuracy and reproducibility of analyses (Yeghicheyan et al., 2019).

2.7. Statistical Methods

Data analysis including linear regression was performed in R (R Core Team, 2020) and visualized using the ggplot2 package (Wickham, 2016). Principal Component Analysis (PCA) of the river samples according to their DOM composition and geochemical concentrations was conducted with the factoextra package in R (Kassambara & Mundt, 2020). Spearman correlations between principal component scores and landcover variables were calculated for each sample using the psych package in R (Revelle, 2024). Spearman correlations between the relative abundance of individual DOM formulae found in all samples and principal component scores were also conducted using similar methodology in R. Significantly correlated molecular formulae were only considered if they had a false discovery rate corrected p-value ($p < 0.05$; Benjamini & Hochberg, 1995). Redundancy analysis (RDA) was conducted in R using the vegan package (Oksanen et al., 2024) to investigate the relationship between the DOM composition (Y matrix, response) and geochemical concentrations (X matrix, explanatory). DOM variables were Hellinger transformed prior to analysis. To simplify the model, colinear geochemical variables were identified and omitted using a step function and further validated using variance inflation factors (VIF < 20).

3. Results

3.1. Water Quality

Water quality parameters are summarized by season in Table 1. Mean water temperature in the MRO rivers ranged from 0.2 to 22.0°C with the lowest average values in March and the highest values in June. The mean water temperature for the Taz tributaries in August was within the range for the MRO rivers in September (10.9°C). Similarly, mean O_2 ranged from 34.1% to 82.0% with the lowest average values in March and the highest in June. The mean O_2 for the Taz tributaries exceeded the range for the MRO rivers (94.4%). In contrast, SpC and DIC generally decreased from March (489 µS cm^{-1}, 68.7 mg L^{-1}) to September (275 µS cm^{-1}, 31.9 mg L^{-1}) in the MRO rivers, reaching their minima in May. The mean SpC and DIC for the Taz tributaries were lower than in the MRO rivers (46 µS cm^{-1} and 3.6 mg L^{-1}, respectively). Finally, mean pH gradually decreased from March to

Table 1
Mean (±SD) Water Quality and DIC Concentrations of West Siberian Lowland (WSL) Rivers by Sampling Month

	O_2 (% sat.)	pH	SpC (µS cm^{-1})	Water temp (°C)	DIC (mg L^{-1})
March (n = 7)	34.0 ± 21.0	8.0 ± 0.3	489 ± 77	0.2 ± 0.1	68.7 ± 18.6
May (n = 8)	78.0 ± 9.1	7.8 ± 0.2	164 ± 59	1.5 ± 0.8	19.1 ± 6.8
June (n = 8)	87.6 ± 22.0	7.6 ± 0.4	227 ± 112	22.0 ± 4.1	27.7 ± 16.5
September (n = 7)	82.0 ± 5.6	7.6 ± 0.4	275 ± 152	13.8 ± 2.2	31.9 ± 21.2
Taz (n = 5)	94.4 ± 7.0	6.8 ± 0.6	46 ± 21	10.9 ± 0.9	3.6 ± 2.0

Note. Taz River tributaries were sampled in August.

June (8.0–7.6) in the MRO rivers with a similar range to the Taz tributaries (6.8 ± 0.6). These seasonal trends are consistent with previous reports of other WSL rivers (e.g., Perminova et al., 2019; Pokrovsky et al., 2015; Vorobyev et al., 2019, 2022).

3.2. DOC Concentrations and DOM Optical Properties

DOC concentrations and optical properties are presented in Figure 2 by month. DOC concentrations in the MRO rivers increased from their minimum in March (mean: 5.9, range: 3.5–7.9 mg L^{-1}) to September (23.5, 8.9–42.6 mg L^{-1}) with DOC concentrations in the Taz tributaries comparable to June and September MRO rivers (18.3, 13.7–24.7 mg L^{-1}; Figure 2a). Similarly, Napierian absorption at 350 nm, as a proxy for CDOM, followed an analogous pattern with the lowest values in March (6.2, 3.3–8.9 m^{-1}), highest in September (58.4, 13.2–137.1 m^{-1}), and CDOM in the Taz tributaries comparable to June and September MRO rivers (39.7, 27.9–70.0 m^{-1}; Figure 2b). Spectral slopes ($S_{275\text{-}295}$) were steepest in March (0.019, 0.017–0.020 nm^{-1}) and became shallower in May (0.015, 0.013–0.016 nm^{-1}), where they remained relatively stable until September, but notably shallower in the Taz tributaries (0.014, 0.013–0.014 nm^{-1}; Figure 2c). Conversely, in MRO rivers $SUVA_{254}$

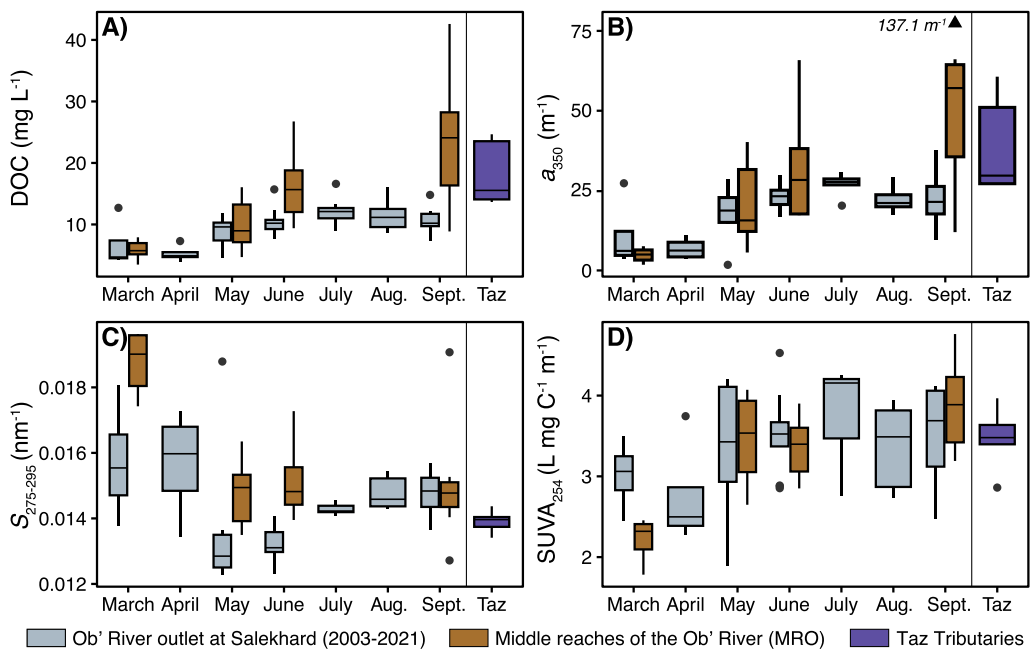

Figure 2. Boxplots of (a) dissolved organic carbon (DOC) concentrations, (b) CDOM absorption at 350 nm (a_{350}), (c) $S_{275\text{-}295}$, and (d) $SUVA_{254}$ of West Siberian Lowland (WSL) rivers by month. Samples are from the middle reaches of the Ob' River (MRO, brown), Taz tributaries in August (purple), as well as past measurements from the Ob' River at Salekhard (light blue) obtained from Arctic GRO (https://arcticgreatrivers.org). Solid vertical lines emphasize geographical separation between MRO rivers and Taz tributaries. Note: DOC concentrations from Salekhard include 2003–2021, while optical data only include 2009–2021. Outlier value outside of the y axis range in panel (b) is labeled and depicted as a triangle.

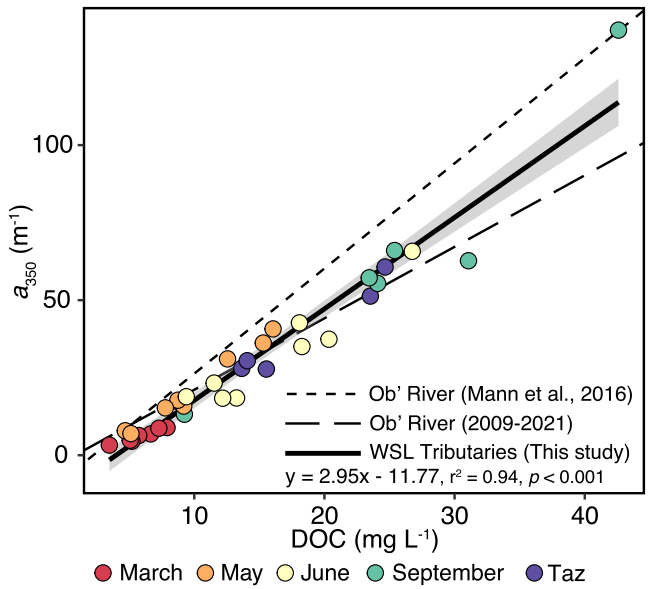

Figure 3. a_{350}-DOC relationship of samples from this study (solid line) compared to past measurements from the Ob' River at Salekhard (short and long dashes). Samples from the middle reaches of the Ob' River (MRO) are colored according to their sampling month including March (red), May (orange), June (yellow), September (green), and Taz tributaries in August (purple). Gray shading represents the 95% confidence interval.

increased from March (2.2, 1.8–2.5 L mg C^{-1} m^{-1}) to May (3.5, 2.6–4.1 L mg C^{-1} m^{-1}) and only slightly increased by September with a similar range of values in the Taz tributaries (3.5, 2.9–4.0 L mg C^{-1} m^{-1}; Figure 2d).

DOC and CDOM ranges were consistent with other tributaries in the WSL (Frey & Smith, 2005; Pokrovsky et al., 2015; Starr et al., 2024), however; summer DOC concentrations were typically higher in MRO rivers than the Ob' mainstem near Tomsk (3–8 mg L^{-1}; Perminova et al., 2019; Pipko et al., 2023). Seasonal trends were similar to the six largest arctic rivers (Ob', Yenisey, Lena, Kolyma, Yukon, Mackenzie), but the WSL rivers had higher DOC concentrations and CDOM in June and September, particularly compared to the Ob' River near the mouth at Salekhard (Behnke et al., 2021; Mann et al., 2016; Spencer et al., 2009; Figures 2a and 2b). Spectral slopes were steeper than the Ob' at Salekhard and most other large arctic rivers (Johnston et al., 2018; Spencer et al., 2009; Figure 2c) with similarity to autochthonous and groundwater-fed North American rivers (0.018–0.024 nm^{-1}; Spencer et al., 2012). In March, $SUVA_{254}$ was lower than several arctic rivers sampled in the winter including the Ob', Yenisey, Lena, Dvina, and Onega (2.5–4.1 L mg C^{-1} m^{-1}; Behnke et al., 2021; Johnston et al., 2018; Mann et al., 2016; Starr et al., 2023), but increased in May-September and remained similar to the Ob' River at Salekhard and the middle reaches (2.9–4.0 mg C^{-1} m^{-1}; Figure 2d; Pipko et al., 2023), as well as smaller Siberian rivers like the Severnaya Dvina, Onega, and Graviyka (3.5–4.2 L mg C^{-1} m^{-1}; Gandois et al., 2021; Johnston et al., 2018; Starr et al., 2023).

DOC concentrations correlated significantly with CDOM across the MRO rivers and Taz tributaries in all seasons ($r^2 = 0.94, p < 0.001$) with similar slopes to the Ob' River at Salekhard from 2009 to 2021 (Figure 3). The a_{350}-DOC slope (2.95) was comparable to the combined slope of the six largest arctic rivers (2.92; Mann et al., 2016), and smaller permafrost-free arctic rivers including the Severnaya Dvina (3.08; Johnston et al., 2018) and Onega River (3.77; Starr et al., 2023). Compared to other major rivers, the a_{350}-DOC slope is steeper than the Columbia River (2.42; Spencer et al., 2012) but shallower than large tropical rivers such as the Congo (3.92) and Ogooué (4.15; Lambert et al., 2015).

3.3. SPE Recovery

DOC recovery via SPE was assessed on five representative river samples from this study (Table S2 in Supporting Information S1). Between 70% and 93% DOC (mean: 78.4%) was retained on PPL columns which is slightly higher than recoveries measured in temperate US wetlands (60%–68%; Kurek et al., 2024), but comparable to recoveries from blackwater rivers and permafrost-fed streams (68%–82%; Yvin et al., 2024). The high recoveries suggest much of the DOM could be retained in the PPL extracts and likely originates from aromatic, terrestrial sources (Yvin et al., 2024). However, we recognize that PPL extracts represent just a fraction of the DOM pool and that the unextracted fraction may contain additional biodegradable compounds, such as hydrophilic species (Grasset et al., 2023; Raeke et al., 2016). Regardless, SPE-DOM is highly comparable across studies and has been shown to vary proportionally with bulk optical and isotopic properties as well as organic S and N across diverse aquatic ecosystems (e.g., Kellerman et al., 2018; Kurek et al., 2020; Poulin et al., 2017).

3.4. DOM Properties Derived From FT-ICR MS Analysis

The relative abundance of compound classes and stoichiometric ratios are presented in Figure 4 and Table S3 in Supporting Information S1 by month. The relative abundance of CA+PPh compounds in MRO rivers increased from their minimum in March (mean: 10.2, range: 9.5%–11.0%) to their max in September (20.6, 15.9–24.8; Figure 4a) with a similar trend in CHO-containing formulae (March: 79.7%, September: 84.2%; Figure S2a in Supporting Information S1). Taz tributary CA+PPh composition was similar to June and September (20.1%, 19.0%–21.8%; Figure 4a) whereas %CHO was lower (82.0%, Figure S2a in Supporting Information S1). $HUP_{Low\ O/C}$ and $HUP_{High\ O/C}$ compounds followed opposite seasonal trends with $HUP_{Low\ O/C}$ decreasing sequentially from March (39.2%, 33.6%–43.3%) to September (25.0%, 19.1%–27.9%; Figure 4b), while

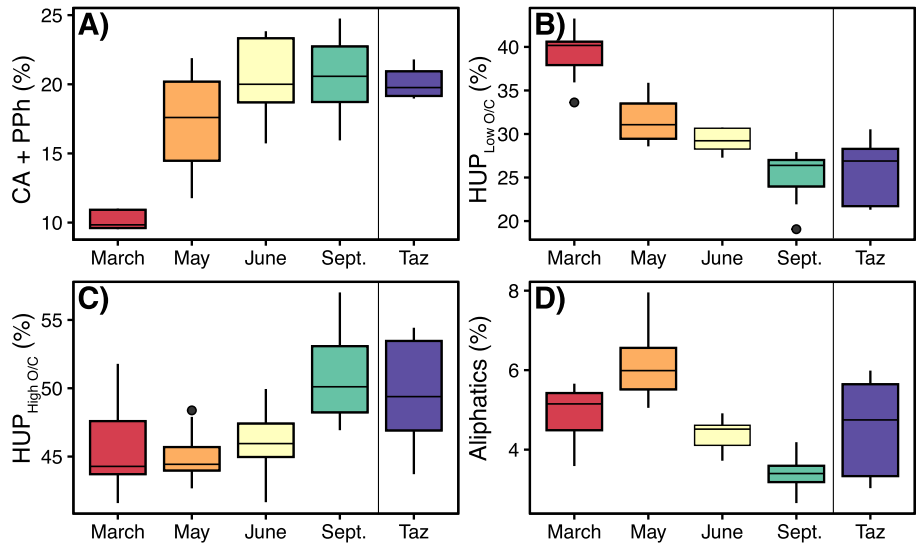

Figure 4. Boxplots of FT-ICR MS compound classes from this study including (a) CA+PPh (condensed aromatic and polyphenolic-like), (b) $HUP_{Low\ O/C}$ (Highly unsaturated and phenolic low O/C), (c) $HUP_{High\ O/C}$ (Highly unsaturated and phenolic high O/C), and (d) Aliphatics (aliphatic-like). Samples from the middle reaches of the Ob' River (MRO) are colored according to their sampling month including March (red), May (orange), June (yellow), September (green), and Taz tributaries in August (purple). Solid vertical lines emphasize geographical separation between MRO rivers and Taz tributaries.

$HUP_{High\ O/C}$ increased from March (45.8%, 41.6%–51.8%) to September (51.0, 46.9–57.0; Figure 4c). The relative abundance of CHON, CHOS, and CHONS-containing formulae followed a pattern analogous to $HUP_{Low\ O/C}$, peaking in March (CHON:13.2, CHOS: 6.0, CHONS: 1.1) and decreasing in September (CHON:11.0, CHOS: 4.2, CHONS: 0.6; Figures S2b–S2d in Supporting Information S1). Taz tributary $HUP_{Low\ O/C}$ and $HUP_{High\ O/C}$ relative abundances were in similar ranges to MRO rivers in September (Figures 4b and 4c), CHON and CHOS were higher than September (Figures S2b and S2c in Supporting Information S1), and CHONS was similar across all months (Figure S2d in Supporting Information S1). Finally, aliphatic-like compounds peaked in May (6.2%, 5.1%–8.0%) and decreased to their minimum in September (3.4%, 2.7%–4.2%) with similar ranges in the Taz tributaries (4.6%, 3.0%–5.9%; Figure 4d).

Both IOS and CARF formulae relative abundance followed $HUP_{Low\ O/C}$ seasonal trends (Figure S3 in Supporting Information S1). IOS and CARF peaked in March (28.7% and 57.4%, respectively) and decreased in May (21.7% and 51.2%, respectively) with Taz tributary values slightly lower than the minima in MRO rivers (19.9% and 49.8%, respectively; Figure S3 in Supporting Information S1). March IOS content was comparable to winter values in the Ob' River at Salekhard (28.2%–30.4%) and marine DOM (30%–33%) but decreased to lower values in May (18%–25%; Figure S3a in Supporting Information S1). In contrast, CARF relative abundance was lower in all seasons than in the Ob' River at Salekhard (64%–70%; Behnke et al., 2021; Figure S3b in Supporting Information S1).

3.5. Geochemistry Groupings and Trends

Several major elements from the MRO rivers and Taz tributaries were analyzed and grouped based on overall seasonal trends (Table S4 in Supporting Information S1). Group 1 consisted of Fe, Al, and P whose median concentrations increased from March to September. In the Taz tributaries, median Fe and Al concentrations were in similar ranges to MRO rivers in September, while P was comparable to concentrations in May and June. Group 2 consisted of Mn and Si whose median concentrations peaked in March, decreased through June, and increased in September. Mn concentrations in the Taz tributaries were in similar ranges to MRO rivers in September while Si was in the same range as in May–June. Group 3 consisted of Na, Ca, and Mg whose median concentrations peaked in March, decreased in May, and then gradually increased through September. Group 3 concentrations in the Taz tributaries were all lower than May MRO concentrations. Finally, median K concentrations peaked in May and were in similar ranges in March, June, and September but much lower in the Taz tributaries. Element

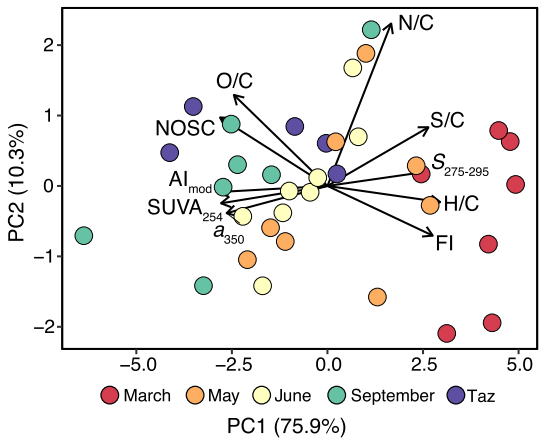

Figure 5. Principal component analysis (PCA) biplot of all samples based on dissolved organic matter composition. Samples from the middle reaches of the Ob' River (MRO) are colored according to their sampling month including March (red), May (orange), June (yellow), September (green), and Taz tributaries in August (purple).

concentrations and trends were comparable to previously values reported across permafrost-free WSL rivers (e.g., Pokrovsky et al., 2015, 2016).

3.6. Ordination Analysis

Optical and FT-ICR MS DOM parameters were summarized and illustrated by the PCA in Figure 5, where 86.2% of the variance could be explained by just two principal components (PC1 and PC2). PC1 (75.9%) correlated positively with aliphatic-like properties ($S_{275\text{-}295}$, H/C), S-content (S/C), and microbial sourcing (FI) and negatively with aromaticity (a_{350}, $SUVA_{254}$, AI_{mod}) with samples separating by sampling month. In contrast, PC2 (10.3%) correlated positively with N-content (N/C) with overlap between all months and the Taz tributaries. Water quality parameters and geochemical concentrations were also summarized and illustrated by the PCA in Figure S4 in Supporting Information S1 with samples clustering by month across both axes.

The relationship between DOM composition and elemental concentrations were investigated using RDA (Figure 6). Model significance was verified using ANOVA ($p < 0.001$) with both axes determined to be significant ($p < 0.001$). Major and trace solute concentrations explained 76.6% of the variance in the DOM variables with 70.0% on the first axis (RDA1) and 6.6% on the second axis (RDA2). Along RDA1 > 0, SpC and DIC clustered with S/C and $S_{275\text{-}295}$ and Si, Mn, and pH with FI and H/C. At RDA1 < 0, DOC and Al clustered with AI_{mod}, O/C, NOSC, $SUVA_{254}$, and a_{350}. Along RDA2 > 0, K clustered with N/C which was opposite of Fe (RDA2 < 0).

4. Discussion

4.1. Seasonality of WSL Rivers

WSL tributaries from the middle reaches of the Ob' River (MRO rivers) experienced dramatic changes in DOM composition and elemental geochemistry from winter (March), spring (May), summer, (June), and early autumn (September; Table 1; Figure 2; Figure 4). Below we discuss the seasonal controls of these trends and their implications for aquatic carbon cycling in this region.

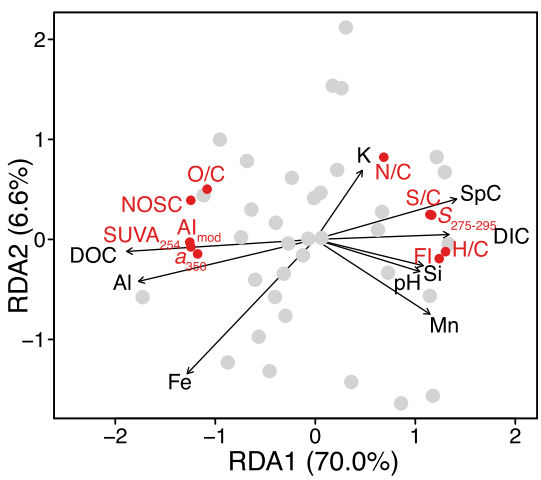

Figure 6. Redundancy analysis (RDA) triplot depicting the variance in dissolved organic matter composition (Principal component analysis from Figure 5, gray points, red points and red text) explained by elemental concentrations and water quality (black text and arrows).

In March, rivers were frozen and effectively disconnected from the surface resulting in low O_2 and high concentrations of DIC, Group 3 elements, and SpC due to ice exclusion and groundwater inputs (Table 1; Table S4 in Supporting Information S1; Pokrovsky et al., 2015; Vorobyev et al., 2019). Low DOC concentrations and CDOM (Figures 2a and 2b), likely originating from groundwater sources, resulted in a slightly shallower a_{350}-DOC slope than the overall Ob' River relationship (Figure 3, red points). This suggests the river exported less CDOM per unit DOC downstream (i.e., $SUVA_{254}$; Figure 2c) which was instead enriched in autochthonous, microbial-like signatures characterized by steeper $S_{275\text{-}295}$ slopes, aliphatic-like compounds, and high N, S-content (Figure 2; Figure 4d; Figure S2 in Supporting Information S1). These molecular signatures likely represented processed and aged DOM as winter DOC in the Ob' River at Salekhard is typically ^{14}C-depleted (Behnke et al., 2021) and high IOS content has also been linked to ^{14}C-depleted DOC in various rivers (Figure S3a in Supporting Information S1; Kellerman et al., 2018). However, enrichment of aliphatic-like and N and S-containing formulae has also been linked to microbial processing and enhanced biolability (Kellerman et al., 2015; Textor et al., 2019), meaning components of this DOM pool could be respired in the Ob' mainstem under favorable thermodynamic conditions (Boye et al., 2017; Valle et al., 2018), particularly as water temperatures increase and surface waters are reoxygenated during ice break-up in the spring.

Spring typically occurs from April to early June, inundating the MRO floodplain and exporting over 50% of all dissolved solutes from the watershed in just 2 months (Krickov et al., 2021; Vorobyev et al., 2019). In May, K concentrations, DOC, CDOM, and CA+PPh compounds all increased (Figure 2; Figure 4a; Table S4 in Supporting Information S1), representing the pulse of terrestrial DOM transported into arctic rivers during periods of greater landscape connectivity driven by meltwater (e.g., Behnke et al., 2021; Holmes et al., 2012; Mann et al., 2016; Raymond et al., 2007). Although much of this terrestrial DOM is aromatic, there was also an increase in the relative abundance of aliphatic-like compounds in May (Figure 4d) representing fresh DOM inputs from leached surface litter and vegetation which are thought to be highly biolabile substrates for respiration (D'Andrilli et al., 2019; Hensgens et al., 2021; Textor et al., 2019). Thus, while CA+PPh compounds are exported downstream to the lower reaches of the Ob' River as CDOM, aliphatic-like compounds are potentially respired upon mixing in the middle reaches, possibly contributing to the higher CO_2 emissions from these regions in the spring and summer compared to continuous permafrost zones (Serikova et al., 2018).

By late June, water temperatures had increased as well as SpC, DIC, and Group 1 element concentrations due to reduced dilution of groundwater baseflow from the passing of peak discharge (Table 1; Table S4 in Supporting Information S1; Pokrovsky et al., 2015; Vorobyev et al., 2019). Mean DOC concentrations and CDOM had also increased from March, illustrating the continual input of terrestrial DOM into WSL tributaries from the surrounding floodplain despite the overall decrease in riverine discharge (Krickov et al., 2021; Vorobyev et al., 2015). However, this DOM was still compositionally similar to DOM from the freshet given their aromaticity and heteroatom content with the main difference being a decrease in aliphatic-like and small relative increase in CA+PPh (Figures 2c and 2d; Figures 4a and 4d; Figure S2 in Supporting Information S1). Such increases in aromatic CA+PPh may enhance CO_2 outgassing from WSL tributaries during the late summer as these highly aromatic compounds sourced from the landscape are typically photolabile, particularly as residence times increase during summer and the region experiences longer exposure to sunlight (Franke et al., 2012; Panneer Selvam et al., 2017). Given sufficiently low discharge conditions and substrate availability, photodegradation of aromatic CA+PPh compounds could increase the proportion of aliphatic-like formulae downstream and contribute significantly to CO_2 fluxes in low-order headwater streams across similar systems (Berggren et al., 2022; Cory et al., 2015; Maavara et al., 2023).

Terrestrial DOM input persisted until early autumn (September) with bulk aromaticity remaining relatively unchanged across the open water period (i.e., $SUVA_{254}$, Figure 2d; CA+PPh, Figure 4a) and instead the relative abundance of $HUP_{High\ O/C}$ and other oxygenated compounds increased (Figure 4c; Table S3 in Supporting Information S1). This suggests a change in the terrestrial DOM sourcing from fresh litter and surface layers from May-June, to more degraded and processed DOM from peat and deeper soil layers in the uplands by the end of summer (September), as also suggested by increases in Group 1 element and Si concentrations (Table S4 in Supporting Information S1; Pokrovsky et al., 2020). Though peak discharge had long passed, these rivers are still connected to the floodplain and prone to high precipitation events that temporarily increase discharge during the autumn (Krickov et al., 2021; Pokrovsky, Manasypov, et al., 2022), effectively flushing DOM out of the surrounding soil layers into the rivers (Starr et al., 2023). Despite relatively low autumn DOC fluxes from this region to downstream (Pokrovsky et al., 2020; Vorobyev et al., 2019), MRO riverine DOM and its extensive floodplain are likely important sources of CDOM to the Ob' River in autumn as northern tributaries from the permafrost zone become disconnected from the landscape when air temperatures decrease.

4.2. Molecular-Level Signatures of WSL Rivers

Seasonality also had a strong impact on the intensity differences of individual DOM formulae across the WSL rivers. Molecular formulae that correlated positively with PC1 scores from Figure 5 were more aliphatic-like (higher H/C), less oxygenated (low O/C), and N and S-enriched compared to negatively correlated formulae (Figure 7a). Given their similarity to the molecular composition of various groundwater systems (e.g., Dvorski et al., 2016; McDonough et al., 2022), the positively correlated formulae therefore illustrate the prevailing signature of groundwater DOM present within river systems (Figure 7b). As the analysis was conducted only with molecular formulae present in every sample, this implies that they are also present during the summer and autumn, though at much lower relative intensities, meaning that they likely represent the baseflow input of groundwater DOM across the WSL rivers. In contrast, negatively correlated formulae are consistent with the DOM composition of surface waters from boreal lakes and streams (e.g., Groeneveld et al., 2020; Hutchins et al., 2017; Kellerman et al., 2015), likely representing the signature of processed aromatic terrestrial inputs through summer

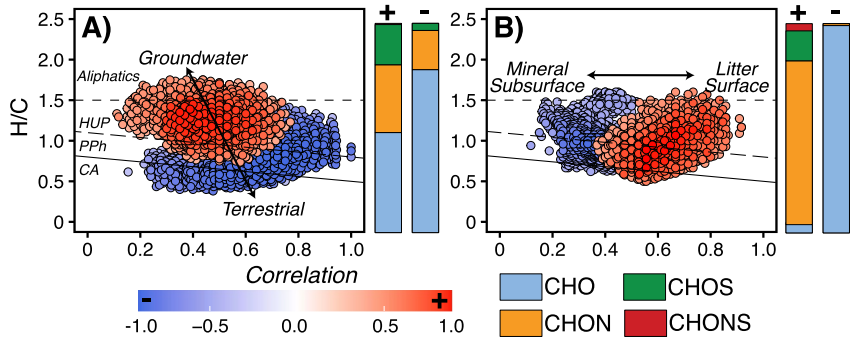

Figure 7. van Krevelen diagrams of spearman correlation coefficients between individual FT-ICR MS formulae and principal component loadings (a) PC1 and (b) PC2 from Figure 5. Positively correlated formulae are colored in red and negatively correlated formulae are in blue. Arrows describe compositional changes of dissolved organic matter (DOM) sourcing from the spearman correlations. Bars describe the heteroatom composition of positively (+) and negatively (−) correlated DOM formulae in each panel and are denoted by CHO (light blue), CHON (orange), CHOS (green), and CHONS (red). Compound class regions are described by dashed/solid lines and include: aliphatics (aliphatic-like), highly unsaturated and phenolic (HUP), polyphenolic-like (PPh), and condensed aromatic-like (CA).

(Figure 7a). Similarly, these formulae illustrate the continuous seepage of soil and peat-derived DOM to the Ob' River even under freezing conditions (Figure 3), as has been suggested in other permafrost-free boreal watersheds influenced by wetlands (e.g., Johnston et al., 2018).

Along RDA1, aliphatic-like and S-enriched DOM properties clustered with SpC, DIC, pH, and Group 2 elements while aromaticity and oxygenation clustered with DOC and Al in the opposite direction (Figure 6). This further illustrates the dependency of microbially-sourced groundwater DOM and terrestrial DOM on seasonality, as well as the cotransport of metals, such as Al, with aromatic DOM from the landscape (Pokrovsky et al., 2016; Pokrovsky, Lim, et al., 2022; Pokrovsky, Manasypov, et al., 2022). While oxygenation generally followed aromaticity, it was also negatively associated with Mn (Figure 6), suggesting that these properties could be related independently of hydrologic sourcing. Oxygen limitation during the winter compels respiring microorganisms to utilize alternate terminal electron acceptors, such as manganese(IV) (oxy)hydroxides, resulting in dissolved winter Mn concentrations that are an order of magnitude greater than the summer (Table S4 in Supporting Information S1; Lovley, 1991; Pokrovsky et al., 2016). Due to thermodynamic constraints, anaerobic respiration selectively oxidizes higher NOSC compounds, removing them from the bulk composition and progressively shifts the remaining DOM pool to lower average NOSC values (Boye et al., 2017; Valle et al., 2018). Formulae with lower oxidation states, such as $HUP_{Low\ O/C}$ compounds, have less electron donating- and accepting capacity, reducing their ability to mediate electron transfer between substrates during anaerobic respiration (Kurek et al., 2023). Therefore, the negative relationship between O/C and NOSC with Mn represents the seasonal effect of redox conditions on WSL river DOM composition, possibly serving as an important control over DOM preservation in other WSL rivers during the winter months.

All formulae significantly correlated with PC2 were similar in aromaticity, occupying the same range of H/C values, but positively correlated formulae were shifted to higher O/C and almost entirely composed of CHON-containing formulae while negatively correlated formulae were shifted to lower O/C ratios and CHO-containing (Figure 7b). Thus, variance along PC2 was driven by the intensity of oxygenated N-containing formulae, representing a specific subset of the bulk DOM. The separation of molecular formulae by O/C is similar to patterns observed in temperate wetlands where formulae that were more abundant in wetland surface waters clustered at O/C > 0.4 and those more abundant in porewaters were shifted to lower O/C values (Kurek et al., 2024). This similar pattern in WSL rivers could suggest that DOM composition is heavily impacted by water interactions with the surface and subsurface. Processes such as leaching from vegetation and surface organic layers afford fresher and more recently processed DOM from van Krevelen regions described as lignin-like and tannin-like (e.g., Allain et al., 2024; Hensgens et al., 2021), while oxygenated and aromatic DOM that passes through clays and minerals adsorb onto surfaces and are removed from the bulk solution (Groeneveld et al., 2020).

K concentrations clustered with N/C along the positive axis of RDA2 and negatively with Fe concentrations, decoupling them from seasonality (Figure 6). While both elements are characteristic of terrestrial sourcing (Krickov et al., 2020; Pokrovsky et al., 2015, 2016), their divergent relationship with N/C further demonstrates the influence of soil and litter layers on riverine DOM composition. High K concentrations suggest plant litter and vegetation leaching from shallow surface layers, such as during the spring freshet (Pokrovsky et al., 2015), while Fe is typically sourced from subsurface mineral horizons (Pokrovsky et al., 2016). Therefore, the partitioning of terrestrial sources between surface litter layers and subsurface mineral soils could account for the variance in molecular-level DOM composition during the open water period (Figure 7b). Differences in sourcing likely impacts downstream DOM biolability and fluvial CO_2 emissions across this region (Krickov et al., 2024; Serikova et al., 2018, 2019) with fresh terrestrial material considered to be highly bioavailable on short times scales (Lapierre & Del Giorgio, 2014).

Interestingly, the DOM composition of the Taz tributaries was similar to the MRO rivers in June-September (Figure 5) rather than clustering separately despite the differences in elemental geochemistry and landcover between the two regions (Figure S4 in Supporting Information S1; Krickov et al., 2024; Pokrovsky, Lim, et al., 2022; Pokrovsky, Manasypov, et al., 2022). The Taz tributaries were comparable in aromaticity and oxygenation to MRO rivers from the same season, but slightly more enriched in N and S-containing formulae (Figure 5; Figure S2 in Supporting Information S1). This is likely due to the influence of continuous permafrost in these watersheds (Drake, Guillemette, et al., 2018; Moore et al., 2023); however, permafrost DOM is typically enriched in aliphatic-like formulae, the lack of which suggests that many of these compounds were rapidly mineralized in headwaters during transport in the early summer (Guillemette et al., 2017; Rogers et al., 2021; Spencer et al., 2015). Furthermore, the clustering of Taz tributaries with MRO rivers in the summer and autumn suggests that despite their geographical separation, WSL rivers are continuously supplied with a pool of aromatic DOM that is compositionally similar between subsurface soil layers and permafrost at maximum thaw. Previous findings reported latitude as the main control over DOC concentrations rather than seasonality in these regions (Pokrovsky et al., 2015; Pokrovsky, Lim, et al., 2022). Here, we demonstrate that seasonality may be more important than latitude or permafrost extent for determining the molecular-level DOM composition, at least within the context of the late summer and early autumn. It is likely that the composition of DOM exported from these regions into the Ob' mainstem may vary from the spring melt through the open water period due to sourcing and latitudinal differences; however, by late summer their properties become similar reflecting common degradation pathways, mineral-water interactions, and homogenization in small headwater streams. Sampling across larger permafrost gradients and multiannual timescales may provide additional insight into these degradation pathways and the relative contributions between the surface layers and subsurface soil in high-latitude arctic rivers.

4.3. Landscape Controls on Riverine DOM Composition

Over 10% of the variance in WSL river DOM composition (PC2) was impacted by terrestrial sourcing driven by individual rivers and land use of each watershed (Figure 5; Table 2), suggesting that surrounding landcover also contributes to WSL river DOM composition and organic C sourcing to the Arctic Ocean. Watershed area had a negative relationship with PC2 DOM scores; however, this relationship is largely due to the Taz tributaries being on average smaller than the MRO rivers (Table S1 in Supporting Information S1), and instead likely reflects the differences in N-content of permafrost watersheds as discussed in Section 4.2. Furthermore, previous studies have reported varying significance of watershed size on carbon dynamics across this region and instead determined landcover to be more significant (e.g., Krickov et al., 2023, 2024; Pokrovsky et al., 2015).

Indeed, peatland coverage correlated negatively with DOM PC2 and overall N-content (Figure S5 in Supporting Information S1), similar to findings in other WSL rivers (Starr et al., 2024). Aromatic DOM properties also increased with peatland coverage, though only in June-September, while %CHON decreased across all seasons (Figure S5 in Supporting Information S1). We also observed minimal impacts of peatland coverage on DOM composition in the continuous permafrost zone, even at maximum summer thaw, highlighting the dominant role of permafrost in carbon transport across northern regions (Starr et al., 2023). This indicates that non-permafrost watersheds with a greater percentage of peatland coverage export more aromatic DOM during summer low flow, with typically less organic N throughout regardless of season. As northern peatlands represent a massive source of vulnerable carbon (Hugelius et al., 2020), this could indicate an important pathway for terrestrial carbon mobilization in arctic rivers, particularly as permafrost landscapes thaw and become influenced by inundated peatlands. These landscapes are an important source of DOC (Frey & Smith, 2005) and terrestrial DOM to large

Table 2
Significant Spearman Correlations Between Landcover and PC2 Scores From Figure 5

	rho	*p*
Watershed area (log-transformed)	−0.62	6.5×10^{-5}
% Mixed forest	−0.37	0.04
% Peatland	−0.51	0.002
% Broadleaf forest	0.63	2.0×10^{-4}
% Light needleleaf forest	−0.72	8.3×10^{-6}
% Dark needleleaf forest	−0.82	3.6×10^{-8}
Needleaf:Broadleaf	−0.79	2.2×10^{-7}

arctic rivers across high-latitude systems (Amon et al., 2012; Gandois et al., 2021; Kaiser, Benner, & Amon, 2017; Rosset et al., 2022). However, due to its high aromaticity and low N-content, this exported organic matter is not likely immediately biolabile and instead could be degraded on longer timescales in coastal systems and in the Arctic Ocean influencing heat transfer and carbon storage (Hansell et al., 2004; Kaiser, Benner, & Amon, 2017; Opsahl et al., 1999).

Despite the importance of peatlands, correlations with peatland coverage were weaker than with forest cover, and we identify a strong negative correlation between the ratio of the combined needleleaf forests to broadleaf forests with PC2 (Needleaf:Broadleaf; Table 2). Furthermore, we find a similar positive trend between aromatic DOM properties and Needleaf:Broadleaf in June–September in addition to a decreasing trend with %CHON across all seasons (Figure S6 in Supporting Information S1). This suggests that during the open water period when rivers are connected to the landscape, watersheds with greater proportions of needleleaf forests export more aromatic and N-depleted DOM than those with more broadleaf forest cover. Conversely, DOM is more enriched in N-containing molecular formulae in rivers whose watersheds contain greater broadleaf forest coverage than needleleaf forests in all seasons, highlighting the important role of soils and the subsurface for DOM processing in these rivers (Figures 7b and 7d).

Past studies have also reported differences between organic matter sourced from coniferous and deciduous forests. For instance, mobile DOM fractions from soils in coniferous forests had higher $SUVA_{254}$ values than from deciduous forests where the immobile organic matter was more aromatic (Jaffrain et al., 2007). Similarly, DOM from coniferous headwaters were enriched in terrestrial fluorophores and had higher molecular weights than DOM from deciduous forests (Cuss & Guéguen, 2015); however, coniferous DOM leaches have also been identified as less biologically reactive than DOM from deciduous leachates (Hensgens et al., 2021). This could suggest that the DOM signatures exported from arctic rivers with lower Needleaf:Broadleaf ratios are more biolabile and may also account for some of the large differences in CO_2 fluxes reported in rivers across the WSL (Krickov et al., 2024; Serikova et al., 2018). However, biolability varies by plant species (Allain et al., 2024; D'Andrilli et al., 2019) and the impact of composition on aquatic carbon cycling is still largely unknown as these molecular signatures represent diverse mixtures of leachates and soils with few studies directly addressing biodegradation in high-latitude arctic systems. Regardless, we demonstrate that the ratio of needleleaf to broadleaf forest cover could be an important control over DOM composition and biolability in WSL rivers and future arctic river studies should consider this relationship as warming-induced landscape changes are actively changing flow paths and hydrologic connectivity.

4.4. Impacts of Landscape Change to WSL Riverine DOM

Warming soils and longer summer seasons will increase the active layer depth in permafrost regions and push the permafrost boundary northward, releasing large stores of soil carbon (Miner et al., 2022; Romanovsky et al., 2010; Schuur et al., 2015). Past studies have hypothesized how shifting permafrost boundaries will impact geochemical concentrations and greenhouse gas fluxes across these regions (e.g., Krickov et al., 2024; Pokrovsky et al., 2015, 2016; Pokrovsky, Lim, et al., 2022; Pokrovsky, Manasypov, et al., 2022; Serikova et al., 2018), and we explore related impacts on DOC and DOM composition within the Taz tributaries. On short timescales, low-order tributaries will receive greater contributions of permafrost-derived DOM into headwaters characterized by greater biolability from aliphatic-like and N,S-enriched formulae (Rogers et al., 2021; Spencer et al., 2015). Though the relative abundance of these formulae is currently greater in the Taz tributaries than the MRO rivers, further warming may increase their proportion, similar to what has been observed in thermokarst thaw slumps and Yedoma thaw (12.8 ± 5.4%; Moore et al., 2023; Drake, Guillemette, et al., 2018; Drake, Raymond, & Spencer, 2018). As continued warming expands active layers and saturates pore spaces, rapid mineralization of these permafrost-derived DOM signatures will likely lead to increased CO_2 fluxes across northern regions, making them comparable to current emissions from rivers in sporadic and permafrost-free zones (Krickov et al., 2024; Serikova et al., 2018). Northern rivers will also become more hydrologically connected to the landscape over time (Ala-aho et al., 2018) and likely mobilize more DOM from the extensive peatlands of the WSL, increasing overall export of DOC and CDOM to the Arctic Ocean (Drozdova et al., 2021; Frey &

Smith, 2005; Rosset et al., 2022; Starr et al., 2024). Greater CDOM delivery into arctic coastal systems could increase mineralization via photodegradation and have ramifications for surface heat transfer as well as Arctic Ocean productivity (Hancke et al., 2012; Hill, 2008; Osburn et al., 2009).

Northern tree line expansion and arctic greening will also impact Siberian tundra and taiga landscapes, changing the distribution of surface vegetation and litter layers (Berner et al., 2020; Forbes et al., 2010; Miles & Esau, 2016). As coniferous forests migrate northward, connected watersheds will likely become more aromatic, driven by an increase of CA+PPh compounds delivered from surface soils as well as an expansion of flow paths to surrounding vegetation (Catalán et al., 2024; Rantala et al., 2016). Bulk parameters such as CDOM and $SUVA_{254}$ will likely increase and become comparable to mean values from the MRO rivers in autumn (Figures 2b and 2d). Furthermore, this shift to aromatic DOM may decrease overall short-term DOM biolability in connected waters (Catalán et al., 2024; Guillemette et al., 2013; Koehler et al., 2012) but conversely may make it more susceptible to photodegradation during transport and in receiving ecosystems (Cory et al., 2015; Franke et al., 2012; Panneer Selvam et al., 2017). However, it is important to note that these rivers will also receive greater inputs from the subsurface and groundwater due to active layer expansion (Frey & McClelland, 2009; Xu et al., 2020), likely increasing the contribution of DIC and decreasing DOC to the overall carbon export (Pokrovsky, Lim, et al., 2022; Pokrovsky, Manasypov, et al., 2022). Increase of active layer thickness will likely enhance delivery of labile, low molecular weight DOM from dispersed peat ice, which contains high proportion of easily degradable carboxylic acids (Kuzmina et al., 2022; Lim et al., 2020, 2022). In contrast, groundwater input will increase the contribution of aged DOM in northern rivers, including low O/C and IOS compounds (Figure S3a and Table S3 in Supporting Information S1), which are typically more biostable on short timescales (Kellerman et al., 2018; Lechtenfeld et al., 2014). Therefore, the overall DOM composition of northern rivers and its impact on carbon cycling will likely reflect a combination of surface and subsurface expansion with specific impacts dependent on hydrology, peatland extent, and dominant vegetation.

Finally, changes to the WSL rivers are likely to be driven by both anthropogenic disturbances, such as deforestation, wildfires, resource extraction, and changes to precipitation (Kirpotin et al., 2021; Kühling et al., 2016; Sada et al., 2019; Xu et al., 2020). Though these disturbances are regional and the overall impact on WSL rivers is largely unknown, we can surmise that the coverage of peatlands and forests may change in these watersheds and have downstream effects on carbon cycling. Much of the agricultural land in this region was abandoned in the 1990s and transitioned to grasslands; however, large portions have been reclaimed and converted to cropland in recent decades (Ivanov et al., 2022; Kühling et al., 2016). Wetland drainage and forest conversion to croplands and grasslands will likely mobilize large pools of organic carbon from the soil into connected rivers. This will shift the composition of exported DOM from highly aromatic and biostable on short timescales, to DOM that is more aliphatic-like, N-enriched, and biolabile (Drake et al., 2019; Spencer et al., 2019; Wilson & Xenopoulos, 2009). Additionally, the overall discharge from the Ob' River has been increasing this century; however, projected DOC fluxes to the Arctic Ocean are unclear, reflecting a combination of increased groundwater contribution and DOC loss from wildfires and mineralization (Kicklighter et al., 2013; Li et al., 2019; Rodríguez-Cardona et al., 2020). The Ob' River has also experienced expansion of the ice-free season and increased winter precipitation, causing the spring freshet to occur earlier in the year with greater intensity (Sada et al., 2019; Xu et al., 2020). As much of the DOM transported from the landscape during peak discharge is fresh and biolabile (Figure 4d), the relative abundance of aliphatic-like formulae in these rivers may increase with peak discharge during the spring, promoting mineralization during transport to the costal Arctic Ocean (Behnke et al., 2021; Kaiser, Canedo-Oropeza, et al., 2017).

In summary, despite the enormous size and importance of the Ob' River floodplain, it has received considerably less attention than other large wetland systems (e.g., Amazon, Congo) with respect to how land use changes will impact carbon dynamics. Our work uncovers baseline trends in seasonal and spatial riverine DOM composition across the WSL and identifies areas for future work to address how changing land cover will impact seasonal carbon export and processing across this region.

5. Conclusion

This study investigated the DOM composition of WSL rivers from the middle reaches of the Ob' River (MRO rivers) with respect to both seasonal and spatial patterns. We report several comparable patterns in DOC and DOM optical properties between large arctic rivers and smaller permafrost-free Siberian rivers. DOC, CDOM,

and molecular-level aromaticity increased in MRO rivers from winter (March) through early autumn (September), representing the transition from groundwater-sourced DOM to terrestrial sources. Furthermore, molecular-level DOM signatures revealed additional differences in terrestrial sourcing between surface litter layers in the spring freshet and deeper subsurface soil layers in early autumn as well as the role of redox processes influencing DOM cycling in winter. These results suggest that seasonality was the main control over DOM composition and export across the sampled rivers. We also identified secondary spatial patterns across the MRO rivers, particularly between the tributaries of the Taz River in the continuous permafrost zone. Taz River tributaries were compositionally similar to MRO rivers in the summer and autumn with respect to aromaticity but had a greater relative abundance of N and S-containing formulae, likely derived from permafrost inputs. Differences between DOM aromaticity and organic N-content across individual watersheds also varied with landcover, such as peatland, forest coverage, and the ratio of needleleaf to broadleaf forests. As high-latitude arctic systems experience warming, changes to precipitation patterns, and anthropogenic disturbances, seasonal and spatial trends in WSL river DOM export will likely respond. Landscape changes will mobilize new biolabile carbon pools from disturbances such as permafrost thaw, while changes to seasonal delivery will probably amplify the terrestrial pulse during the spring freshet, both having ramifications for coastal export and aquatic greenhouse gas emissions.

Conflict of Interest

The authors declare no conflicts of interest relevant to this study.

Data Availability Statement

The authors declare that all data supporting the results of this study have been uploaded as supporting Data Set S1 in the supplemental information. All FT-ICR MS spectra, assigned molecular formulae associated with this study, and Data Set S1 are also archived in the Open Science Framework (Kurek, 2024; https://doi.org/10.17605/OSF.IO/Q42DW).

Acknowledgments
R.G.M.S. acknowledges support from the NSF Belmont Forum Award #2124464. O.P. acknowledges support from TSU Programme Priority-2030 and project PEACE of PEPR FairCarboN ANR-22-PEXF-0011. A portion of this work was performed at the National High Magnetic Field Laboratory ICR User Facility, which is supported by the National Science Foundation Division of Chemistry and Division of Materials Research through DMR-2128556 and the state of Florida.

References

Ala-aho, P., Soulsby, C., Pokrovsky, O. S., Kirpotin, S. N., Karlsson, J., Serikova, S., et al. (2018). Using stable isotopes to assess surface water source dynamics and hydrological connectivity in a high-latitude wetland and permafrost influenced landscape. *Journal of Hydrology*, *556*, 279–293. https://doi.org/10.1016/j.jhydrol.2017.11.024

Allain, A., Alexis, M. A., Bridoux, M. C., Shirokova, L. S., Payandi-Rolland, D., Pokrovsky, O. S., & Rouelle, M. (2024). The specific molecular signature of dissolved organic matter extracted from different arctic plant species persists after biodegradation. *Soil Biology and Biochemistry*, *193*, 109393. https://doi.org/10.1016/j.soilbio.2024.109393

Amon, R. M. W., Rinehart, A. J., Duan, S., Louchouarn, P., Prokushkin, A., Guggenberger, G., et al. (2012). Dissolved organic matter sources in large Arctic rivers. *Geochimica et Cosmochimica Acta*, *94*, 217–237. https://doi.org/10.1016/j.gca.2012.07.015

Battin, T. J., Luyssaert, S., Kaplan, L. A., Aufdenkampe, A. K., Richter, A., & Tranvik, L. J. (2009). The boundless carbon cycle. *Nature Geoscience*, *2*(9), 598–600. https://doi.org/10.1038/ngeo618

Begum, M. S., Park, J.-H., Yang, L., Shin, K. H., & Hur, J. (2023). Optical and molecular indices of dissolved organic matter for estimating biodegradability and resulting carbon dioxide production in inland waters: A review. *Water Research*, *228*, 119362. https://doi.org/10.1016/j.watres.2022.119362

Behnke, M. I., McClelland, J. W., Tank, S. E., Kellerman, A. M., Holmes, R. M., Haghipour, N., et al. (2021). Pan-Arctic riverine dissolved organic matter: Synchronous molecular stability, shifting sources and subsidies. *Global Biogeochemical Cycles*, *35*(4), e2020GB006871. https://doi.org/10.1029/2020GB006871

Benjamini, Y., & Hochberg, Y. (1995). Controlling the false discovery rate: A practical and powerful approach to multiple testing. *Journal of the Royal Statistical Society. Series B (Methodological)*, *57*(1), 289–300. https://doi.org/10.1111/j.2517-6161.1995.tb02031.x

Berggren, M., Guillemette, F., Bieroza, M., Buffam, I., Deininger, A., Hawkes, J. A., et al. (2022). Unified understanding of intrinsic and extrinsic controls of dissolved organic carbon reactivity in aquatic ecosystems. *Ecology*, *103*(9), e3763. https://doi.org/10.1002/ecy.3763

Berner, L. T., Massey, R., Jantz, P., Forbes, B. C., Macias-Fauria, M., Myers-Smith, I., et al. (2020). Summer warming explains widespread but not uniform greening in the Arctic tundra biome. *Nature Communications*, *11*(1), 4621. https://doi.org/10.1038/s41467-020-18479-5

Boye, K., Noël, V., Tfaily, M. M., Bone, S. E., Williams, K. H., Bargar, J. R., & Fendorf, S. (2017). Thermodynamically controlled preservation of organic carbon in floodplains. *Nature Geoscience*, *10*(6), 415–419. https://doi.org/10.1038/ngeo2940

Catalán, N., Marcé, R., Kothawala, D. N., & Tranvik, L. J. (2016). Organic carbon decomposition rates controlled by water retention time across inland waters. *Nature Geoscience*, *9*(7), 501–504. https://doi.org/10.1038/ngeo2720

Catalán, N., Rofner, C., Verpoorter, C., Pérez, M. T., Dittmar, T., Tranvik, L., et al. (2024). Treeline displacement may affect lake dissolved organic matter processing at high latitudes and altitudes. *Nature Communications*, *15*(1), 2640. https://doi.org/10.1038/s41467-024-46789-5

Cole, J. J., Prairie, Y. T., Caraco, N. F., McDowell, W. H., Tranvik, L. J., Striegl, R. G., et al. (2007). Plumbing the global carbon cycle: Integrating inland waters into the terrestrial carbon budget. *Ecosystems*, *10*(1), 172–185. https://doi.org/10.1007/s10021-006-9013-8

Corilo, Y. (2014). PetroOrg [Computer software]. Retrieved from https://www.research.fsu.edu/research-offices/oc/technologies/petroorg-software

Cory, R. M., Harrold, K. H., Neilson, B. T., & Kling, G. W. (2015). Controls on dissolved organic matter (DOM) degradation in a headwater stream: The influence of photochemical and hydrological conditions in determining light-limitation or substrate-limitation of photo-degradation. *Biogeosciences*, *12*(22), 6669–6685. https://doi.org/10.5194/bg-12-6669-2015

Cory, R. M., & McKnight, D. M. (2005). Fluorescence spectroscopy reveals ubiquitous presence of oxidized and reduced quinones in dissolved organic matter. *Environmental Science & Technology*, *39*(21), 8142–8149. https://doi.org/10.1021/es0506962

Cuss, C. W., & Guéguen, C. (2015). Relationships between molecular weight and fluorescence properties for size-fractionated dissolved organic matter from fresh and aged sources. *Water Research*, *68*, 487–497. https://doi.org/10.1016/j.watres.2014.10.013

D'Andrilli, J., Junker, J. R., Smith, H. J., Scholl, E. A., & Foreman, C. M. (2019). DOM composition alters ecosystem function during microbial processing of isolated sources. *Biogeochemistry*, *142*(2), 281–298. https://doi.org/10.1007/s10533-018-00534-5

Davy, R., & Outten, S. (2020). The Arctic surface climate in CMIP6: Status and developments since CMIP5. *Journal of Climate*, *33*(18), 8047–8068. https://doi.org/10.1175/JCLI-D-19-0990.1

Dittmar, T., Koch, B., Hertkorn, N., & Kattner, G. (2008). A simple and efficient method for the solid-phase extraction of dissolved organic matter (SPE-DOM) from seawater. *Limnology and Oceanography: Methods*, *6*(6), 230–235. https://doi.org/10.4319/lom.2008.6.230

Drake, T. W., Guillemette, F., Hemingway, J. D., Chanton, J. P., Podgorski, D. C., Zimov, N. S., & Spencer, R. G. M. (2018). The ephemeral signature of permafrost carbon in an Arctic fluvial network. *Journal of Geophysical Research: Biogeosciences*, *123*(5), 1475–1485. https://doi.org/10.1029/2017JG004311

Drake, T. W., Raymond, P. A., & Spencer, R. G. M. (2018). Terrestrial carbon inputs to inland waters: A current synthesis of estimates and uncertainty. *Limnology and Oceanography Letters*, *3*(3), 132–142. https://doi.org/10.1002/lol2.10055

Drake, T. W., Van Oost, K., Barthel, M., Bauters, M., Hoyt, A. M., Podgorski, D. C., et al. (2019). Mobilization of aged and biolabile soil carbon by tropical deforestation. *Nature Geoscience*, *12*(7), 541–546. https://doi.org/10.1038/s41561-019-0384-9

Drozdova, A. N., Nedospasov, A. A., Lobus, N. V., Patsaeva, S. V., & Shchuka, S. A. (2021). CDOM optical properties and DOC content in the largest mixing zones of the Siberian shelf seas. *Remote Sensing*, *13*(6), 1145. https://doi.org/10.3390/rs13061145

Dvorski, S. E.-M., Gonsior, M., Hertkorn, N., Uhl, J., Müller, H., Griebler, C., & Schmitt-Kopplin, P. (2016). Geochemistry of dissolved organic matter in a spatially highly resolved groundwater petroleum hydrocarbon plume cross-section. *Environmental Science & Technology*, *50*(11), 5536–5546. https://doi.org/10.1021/acs.est.6b00849

Forbes, B. C., Fauria, M. M., & Zetterberg, P. (2010). Russian Arctic warming and 'greening' are closely tracked by tundra shrub willows. *Global Change Biology*, *16*(5), 1542–1554. https://doi.org/10.1111/j.1365-2486.2009.02047.x

Franke, D., Hamilton, M. W., & Ziegler, S. E. (2012). Variation in the photochemical lability of dissolved organic matter in a large boreal watershed. *Aquatic Sciences*, *74*(4), 751–768. https://doi.org/10.1007/s00027-012-0258-3

Frey, K. E., & McClelland, J. W. (2009). Impacts of permafrost degradation on arctic river biogeochemistry. *Hydrological Processes*, *23*(1), 169–182. https://doi.org/10.1002/hyp.7196

Frey, K. E., Siegel, D. I., & Smith, L. C. (2007). Geochemistry of west Siberian streams and their potential response to permafrost degradation. *Water Resources Research*, *43*(3), W03406. https://doi.org/10.1029/2006WR004902

Frey, K. E., & Smith, L. C. (2005). Amplified carbon release from vast West Siberian peatlands by 2100. *Geophysical Research Letters*, *32*(9), 2004GL022025. https://doi.org/10.1029/2004GL022025

Gandois, L., Tananaev, N. I., Prokushkin, A., Solnyshkin, I., & Teisserenc, R. (2021). Seasonality of DOC export from a Russian subarctic catchment underlain by discontinuous permafrost, highlighted by high-frequency monitoring. *Journal of Geophysical Research: Biogeosciences*, *126*(10), e2020JG006152. https://doi.org/10.1029/2020JG006152

Gorham, E. (1991). Northern peatlands: Role in the carbon cycle and probable responses to climatic warming. *Ecological Applications*, *1*(2), 182–195. https://doi.org/10.2307/1941811

Grasset, C., Groeneveld, M., Tranvik, L. J., Robertson, L. P., & Hawkes, J. A. (2023). Hydrophilic species are the most biodegradable components of freshwater dissolved organic matter. *Environmental Science & Technology*, *57*(36), 13463–13472. https://doi.org/10.1021/acs.est.3c02175

Groeneveld, M., Catalán, N., Attermeyer, K., Hawkes, J., Einarsdóttir, K., Kothawala, D., et al. (2020). Selective adsorption of terrestrial dissolved organic matter to inorganic surfaces along a boreal inland water continuum. *Journal of Geophysical Research: Biogeosciences*, *125*(3), e2019JG005236. https://doi.org/10.1029/2019JG005236

Guillemette, F., Bianchi, T. S., & Spencer, R. G. M. (2017). Old before your time: Ancient carbon incorporation in contemporary aquatic foodwebs. *Limnology and Oceanography*, *62*(4), 1682–1700. https://doi.org/10.1002/lno.10525

Guillemette, F., McCallister, S. L., & Del Giorgio, P. A. (2013). Differentiating the degradation dynamics of algal and terrestrial carbon within complex natural dissolved organic carbon in temperate lakes. *Journal of Geophysical Research: Biogeosciences*, *118*(3), 963–973. https://doi.org/10.1002/jgrg.20077

Hancke, K., Hovland, E. K., Volent, Z., Pettersen, R., Johnsen, G., Moline, M., & Sakshaug, E. (2012). Optical properties of CDOM across the Polar Front in the Barents Sea: Origin, distribution and significance. *Journal of Marine Systems*, *130*, 219–227. https://doi.org/10.1016/j.jmarsys.2012.06.006

Hansell, D. A., Kadko, D., & Bates, N. R. (2004). Degradation of terrigenous dissolved organic carbon in the western Arctic Ocean. *Science*, *304*(5672), 858–861. https://doi.org/10.1126/science.1096175

Helms, J. R., Stubbins, A., Ritchie, J. D., Minor, E. C., Kieber, D. J., & Mopper, K. (2008). Absorption spectral slopes and slope ratios as indicators of molecular weight, source, and photobleaching of chromophoric dissolved organic matter. *Limnology and Oceanography*, *53*(3), 955–969. https://doi.org/10.4319/lo.2008.53.3.0955

Hendrickson, C. L., Quinn, J. P., Kaiser, N. K., Smith, D. F., Blakney, G. T., Chen, T., et al. (2015). 21 Tesla Fourier transform ion cyclotron resonance mass spectrometer: A national resource for ultrahigh resolution mass analysis. *Journal of the American Society for Mass Spectrometry*, *26*(9), 1626–1632. https://doi.org/10.1007/s13361-015-1182-2

Hensgens, G., Lechtenfeld, O. J., Guillemette, F., Laudon, H., & Berggren, M. (2021). Impacts of litter decay on organic leachate composition and reactivity. *Biogeochemistry*, *154*(1), 99–117. https://doi.org/10.1007/s10533-021-00799-3

Hill, V. J. (2008). Impacts of chromophoric dissolved organic material on surface ocean heating in the Chukchi Sea. *Journal of Geophysical Research*, *113*(C7), C07024. https://doi.org/10.1029/2007JC004119

Holmes, R. M., McClelland, J. W., Peterson, B. J., Tank, S. E., Bulygina, E., Eglinton, T. I., et al. (2012). Seasonal and annual fluxes of nutrients and organic matter from large rivers to the Arctic Ocean and surrounding seas. *Estuaries and Coasts*, *35*(2), 369–382. https://doi.org/10.1007/s12237-011-9386-6

Hugelius, G., Loisel, J., Chadburn, S., Jackson, R. B., Jones, M., MacDonald, G., et al. (2020). Large stocks of peatland carbon and nitrogen are vulnerable to permafrost thaw. *Proceedings of the National Academy of Sciences*, *117*(34), 20438–20446. https://doi.org/10.1073/pnas.1916387117

Hugelius, G., Strauss, J., Zubrzycki, S., Harden, J. W., Schuur, E. A. G., Ping, C.-L., et al. (2014). Estimated stocks of circumpolar permafrost carbon with quantified uncertainty ranges and identified data gaps. *Biogeosciences*, *11*(23), 6573–6593. https://doi.org/10.5194/bg-11-6573-2014

Hutchins, R. H. S., Aukes, P., Schiff, S. L., Dittmar, T., Prairie, Y. T., & Del Giorgio, P. A. (2017). The optical, chemical, and molecular dissolved organic matter succession along a boreal soil-stream-river continuum. *Journal of Geophysical Research: Biogeosciences*, *122*(11), 2892–2908. https://doi.org/10.1002/2017JG004094

Ivanov, V., Milyaev, I., Konstantinov, A., & Loiko, S. (2022). Land-use changes on Ob River floodplain (Western Siberia, Russia) in context of natural and social changes over past 200 years. *Land*, *11*(12), 2258. https://doi.org/10.3390/land11122258

Jaffrain, J., Gérard, F., Meyer, M., & Ranger, J. (2007). Assessing the quality of dissolved organic matter in forest soils using ultraviolet absorption spectrophotometry. *Soil Science Society of America Journal*, *71*(6), 1851–1858. https://doi.org/10.2136/sssaj2006.0202

Johnston, S. E., Shorina, N., Bulygina, E., Vorobjeva, T., Chupakova, A., Klimov, S. I., et al. (2018). Flux and seasonality of dissolved organic matter from the Northern Dvina (Severnaya Dvina) River, Russia. *Journal of Geophysical Research: Biogeosciences*, *123*(3), 1041–1056. https://doi.org/10.1002/2017JG004337

Kaiser, K., Benner, R., & Amon, R. M. W. (2017). The fate of terrigenous dissolved organic carbon on the Eurasian shelves and export to the North Atlantic. *Journal of Geophysical Research: Oceans*, *122*(1), 4–22. https://doi.org/10.1002/2016JC012380

Kaiser, K., Canedo-Oropeza, M., McMahon, R., & Amon, R. M. W. (2017). Origins and transformations of dissolved organic matter in large Arctic rivers. *Scientific Reports*, *7*(1), 13064. https://doi.org/10.1038/s41598-017-12729-1

Karlsson, J., Serikova, S., Vorobyev, S. N., Rocher-Ros, G., Denfeld, B., & Pokrovsky, O. S. (2021). Carbon emission from Western Siberian inland waters. *Nature Communications*, *12*(1), 825. https://doi.org/10.1038/s41467-021-21054-1

Kassambara, A., & Mundt, F. (2020). factoextra: Extract and visualize the results of multivariate data analyses (Version 1.0.7) [Computer software]. *CRAN*. https://cran.r-project.org/web/packages/factoextra/index.html

Kellerman, A. M., Guillemette, F., Podgorski, D. C., Aiken, G. R., Butler, K. D., & Spencer, R. G. M. (2018). Unifying concepts linking dissolved organic matter composition to persistence in aquatic ecosystems. *Environmental Science & Technology*, *52*(5), 2538–2548. https://doi.org/10.1021/acs.est.7b05513

Kellerman, A. M., Kothawala, D. N., Dittmar, T., & Tranvik, L. J. (2015). Persistence of dissolved organic matter in lakes related to its molecular characteristics. *Nature Geoscience*, *8*(6), 454–457. https://doi.org/10.1038/ngeo2440

Kicklighter, D. W., Hayes, D. J., McClelland, J. W., Peterson, B. J., McGuire, A. D., & Melillo, J. M. (2013). Insights and issues with simulating terrestrial DOC loading of Arctic river networks. *Ecological Applications*, *23*(8), 1817–1836. https://doi.org/10.1890/11-1050.1

Kirpotin, S. N., Callaghan, T. V., Peregon, A. M., Babenko, A. S., Berman, D. I., Bulakhova, N. A., et al. (2021). Impacts of environmental change on biodiversity and vegetation dynamics in Siberia. *Ambio*, *50*(11), 1926–1952. https://doi.org/10.1007/s13280-021-01570-6

Koch, B. P., & Dittmar, T. (2006). From mass to structure: An aromaticity index for high-resolution mass data of natural organic matter. *Rapid Communications in Mass Spectrometry*, *20*(5), 926–932. https://doi.org/10.1002/rcm.2386

Koch, B. P., & Dittmar, T. (2016). From mass to structure: An aromaticity index for high-resolution mass data of natural organic matter. *Rapid Communications in Mass Spectrometry*, *30*(1). 250–250. https://doi.org/10.1002/rcm.7433

Koehler, B., Von Wachenfeldt, E., Kothawala, D., & Tranvik, L. J. (2012). Reactivity continuum of dissolved organic carbon decomposition in lake water. *Journal of Geophysical Research*, *117*(G1), 2011JG001793. https://doi.org/10.1029/2011JG001793

Kremenetski, K. V., Velichko, A. A., Borisova, O. K., MacDonald, G. M., Smith, L. C., Frey, K. E., & Orlova, L. A. (2003). Peatlands of the Western Siberian lowlands: Current knowledge on zonation, carbon content and Late Quaternary history. *Quaternary Science Reviews*, *22*(5), 703–723. https://doi.org/10.1016/S0277-3791(02)00196-8

Krickov, I. V., Lim, A. G., Manasypov, R. M., Loiko, S. V., Vorobyev, S. N., Shevchenko, V. P., et al. (2020). Major and trace elements in suspended matter of western Siberian rivers: First assessment across permafrost zones and landscape parameters of watersheds. *Geochimica et Cosmochimica Acta*, *269*, 429–450. https://doi.org/10.1016/j.gca.2019.11.005

Krickov, I. V., Lim, A. G., Shirokova, L. S., Korets, M. A., Karlsson, J., & Pokrovsky, O. S. (2023). Environmental controllers for carbon emission and concentration patterns in Siberian rivers during different seasons. *Science of The Total Environment*, *859*, 160202. https://doi.org/10.1016/j.scitotenv.2022.160202

Krickov, I. V., Lim, A. G., Shirokova, L. S., Korets, M. A., & Pokrovsky, O. S. (2024). Fluvial carbon dioxide emissions peak at the permafrost thawing front in the Western Siberia Lowland. *Science of The Total Environment*, *936*, 173491. https://doi.org/10.1016/j.scitotenv.2024.173491

Krickov, I. V., Serikova, S., Pokrovsky, O. S., Vorobyev, S. N., Lim, A. G., Siewert, M. B., & Karlsson, J. (2021). Sizable carbon emission from the floodplain of Ob River. *Ecological Indicators*, *131*, 108164. https://doi.org/10.1016/j.ecolind.2021.108164

Kühling, I., Broll, G., & Trautz, D. (2016). Spatio-temporal analysis of agricultural land-use intensity across the Western Siberian grain belt. *Science of The Total Environment*, *544*, 271–280. https://doi.org/10.1016/j.scitotenv.2015.11.129

Kurek, M. (2024). Assessing the molecular-level controls of dissolved organic matter cycling in West Siberian Lowland rivers [Dataset]. *OSF*. https://doi.org/10.17605/OSF.IO/Q42DW

Kurek, M. R., Garcia-Tigreros, F., Nichols, N. A., Druschel, G. K., Wickland, K. P., Dornblaser, M. M., et al. (2023). High voltage: The molecular properties of redox-active dissolved organic matter in northern high-latitude lakes. *Environmental Science & Technology*, *57*(23), 8617–8627. https://doi.org/10.1021/acs.est.3c01782

Kurek, M. R., Poulin, B. A., McKenna, A. M., & Spencer, R. G. M. (2020). Deciphering dissolved organic matter: Ionization, dopant, and fragmentation insights via Fourier transform-ion cyclotron resonance mass spectrometry. *Environmental Science & Technology*, *54*(24), 16249–16259. https://doi.org/10.1021/acs.est.0c05206

Kurek, M. R., Wickland, K. P., Nichols, N. A., McKenna, A. M., Anderson, S. M., Dornblaser, M. M., et al. (2024). Linking dissolved organic matter composition to landscape properties in wetlands across the United States of America. *Global Biogeochemical Cycles*, *38*(5), e2023GB007917. https://doi.org/10.1029/2023GB007917

Kuzmina, D. M., Lim, A. G., Loiko, S. V., Shefer, N., Shirokova, L. S., Julien, F., et al. (2022). Dispersed ice of permafrost peatlands represents an important source of labile carboxylic acids, nutrients and metals. *Geoderma*, *429*, 116256. https://doi.org/10.1016/j.geoderma.2022.116256

Lambert, T., Darchambeau, F., Bouillon, S., Alhou, B., Mbega, J.-D., Teodoru, C. R., et al. (2015). Landscape control on the spatial and temporal variability of chromophoric dissolved organic matter and dissolved organic carbon in large African rivers. *Ecosystems*, *18*(7), 1224–1239. https://doi.org/10.1007/s10021-015-9894-5

Lapierre, J.-F., & Del Giorgio, P. A. (2014). Partial coupling and differential regulation of biologically and photochemically labile dissolved organic carbon across boreal aquatic networks. *Biogeosciences*, *11*(20), 5969–5985. https://doi.org/10.5194/bg-11-5969-2014

Lechtenfeld, O. J., Kattner, G., Flerus, R., McCallister, S. L., Schmitt-Kopplin, P., & Koch, B. P. (2014). Molecular transformation and degradation of refractory dissolved organic matter in the Atlantic and Southern Ocean. *Geochimica et Cosmochimica Acta*, *126*, 321–337. https://doi.org/10.1016/j.gca.2013.11.009

Li, M., Peng, C., Zhou, X., Yang, Y., Guo, Y., Shi, G., & Zhu, Q. (2019). Modeling global riverine DOC flux dynamics from 1951 to 2015. *Journal of Advances in Modeling Earth Systems*, *11*(2), 514–530. https://doi.org/10.1029/2018MS001363

Lim, A. G., Loiko, S. V., Kuzmina, D. M., Krickov, I. V., Shirokova, L. S., Kulizhsky, S. P., et al. (2020). Dispersed ground ice of permafrost peatlands: Potential unaccounted carbon, nutrient and metal sources. *Chemosphere*, *266*, 128953. https://doi.org/10.1016/j.chemosphere.2020.128953

Lim, A. G., Loiko, S. V., Kuzmina, D. M., Krickov, I. V., Shirokova, L. S., Kulizhsky, S. P., & Pokrovsky, O. S. (2022). Organic carbon, and major and trace elements reside in labile low-molecular form in the ground ice of permafrost peatlands: A case study of colloids in peat ice of Western Siberia. *Environmental Science Processes & Impacts*, *24*(9), 1443–1459. https://doi.org/10.1039/d1em00547b

Limpens, J., Berendse, F., Blodau, C., Canadell, J. G., Freeman, C., Holden, J., et al. (2008). Peatlands and the carbon cycle: From local processes to global implications – A synthesis. *Biogeosciences*, *5*(5), 1475–1491. https://doi.org/10.5194/bg-5-1475-2008

Lovley, D. R. (1991). Dissimilatory Fe(III) and Mn(IV) reduction. *Microbiological Reviews*, *55*(2), 259–287. https://doi.org/10.1128/mr.55.2.259-287.1991

Maavara, T., Brinkerhoff, C., Hosen, J., Aho, K., Logozzo, L., Saiers, J., et al. (2023). Watershed DOC uptake occurs mostly in lakes in the summer and in rivers in the winter. *Limnology and Oceanography*, *68*(3), 735–751. https://doi.org/10.1002/lno.12306

Mann, P. J., Spencer, R. G. M., Hernes, P. J., Six, J., Aiken, G. R., Tank, S. E., et al. (2016). Pan-Arctic trends in terrestrial dissolved organic matter from optical measurements. *Frontiers in Earth Science*, *4*, 25. https://doi.org/10.3389/feart.2016.00025

McDonough, L. K., Andersen, M. S., Behnke, M. I., Rutlidge, H., Oudone, P., Meredith, K., et al. (2022). A new conceptual framework for the transformation of groundwater dissolved organic matter. *Nature Communications*, *13*(1), 2153. https://doi.org/10.1038/s41467-022-29711-9

McKnight, D. M., Boyer, E. W., Westerhoff, P. K., Doran, P. T., Kulbe, T., & Andersen, D. T. (2001). Spectrofluorometric characterization of dissolved organic matter for indication of precursor organic material and aromaticity. *Limnology and Oceanography*, *46*(1), 38–48. https://doi.org/10.4319/lo.2001.46.1.0038

Miles, V. V., & Esau, I. (2016). Spatial heterogeneity of greening and browning between and within bioclimatic zones in northern West Siberia. *Environmental Research Letters*, *11*(11), 115002. https://doi.org/10.1088/1748-9326/11/11/115002

Miner, K. R., Turetsky, M. R., Malina, E., Bartsch, A., Tamminen, J., McGuire, A. D., et al. (2022). Permafrost carbon emissions in a changing Arctic. *Nature Reviews Earth & Environment*, *3*(1), 55–67. https://doi.org/10.1038/s43017-021-00230-3

Moore, M. R. N., Tank, S. E., Kurek, M. R., Taskovic, M., McKenna, A. M., Smith, J. L. J., et al. (2023). Ultrahigh resolution dissolved organic matter characterization reveals distinct permafrost characteristics on the Peel Plateau, Canada. *Biogeochemistry*, *167*(2), 99–117. https://doi.org/10.1007/s10533-023-01101-3

Oksanen, J., Simpson, G. L., Blanchet, F. G., Kindt, R., Legendre, P., Minchin, P. R., et al. (2024). vegan: Community Ecology Package (Version 2.6-6.1) [Computer software]. *CRAN*. https://cran.r-project.org/web/packages/vegan/index.html

Olefeldt, D., Roulet, N., Giesler, R., & Persson, A. (2013). Total waterborne carbon export and DOC composition from ten nested subarctic peatland catchments—Importance of peatland cover, groundwater influence, and inter-annual variability of precipitation patterns. *Hydrological Processes*, *27*(16), 2280–2294. https://doi.org/10.1002/hyp.9358

Opsahl, S., Benner, R., & Amon, R. M. W. (1999). Major flux of terrigenous dissolved organic matter through the Arctic Ocean. *Limnology and Oceanography*, *44*(8), 2017–2023. https://doi.org/10.4319/lo.1999.44.8.2017

Osburn, C. L., Retamal, L., & Vincent, W. F. (2009). Photoreactivity of chromophoric dissolved organic matter transported by the Mackenzie River to the Beaufort Sea. *Marine Chemistry*, *115*(1), 10–20. https://doi.org/10.1016/j.marchem.2009.05.003

Panneer Selvam, B., Lapierre, J.-F., Guillemette, F., Voigt, C., Lamprecht, R. E., Biasi, C., et al. (2017). Degradation potentials of dissolved organic carbon (DOC) from thawed permafrost peat. *Scientific Reports*, *7*(1), 45811. https://doi.org/10.1038/srep45811

Payandi-Rolland, D., Shirokova, L. S., Tesfa, M., Bénézeth, P., Lim, A. G., Kuzmina, D., et al. (2020). Dissolved organic matter biodegradation along a hydrological continuum in permafrost peatlands. *Science of The Total Environment*, *749*, 141463. https://doi.org/10.1016/j.scitotenv.2020.141463

Perminova, I. V., Shirshin, E. A., Zherebker, A., Pipko, I. I., Pugach, S. P., Dudarev, O. V., et al. (2019). Signatures of molecular unification and progressive oxidation unfold in dissolved organic matter of the Ob-Irtysh River system along its path to the Arctic Ocean. *Scientific Reports*, *9*(1), 19487. https://doi.org/10.1038/s41598-019-55662-1

Pipko, I. I., Pugach, S. P., Shcherbakova, K. P., & Semiletov, I. P. (2023). Optical signatures of dissolved organic matter in the Siberian Rivers during summer season. *Journal of Hydrology*, *620*, 129468. https://doi.org/10.1016/j.jhydrol.2023.129468

Plaza, C., Pegoraro, E., Bracho, R., Celis, G., Crummer, K. G., Hutchings, J. A., et al. (2019). Direct observation of permafrost degradation and rapid soil carbon loss in tundra. *Nature Geoscience*, *12*(8), 627–631. https://doi.org/10.1038/s41561-019-0387-6

Pokrovsky, O. S., Lim, A. G., Krickov, I. V., Korets, M. A., Shirokova, L. S., & Vorobyev, S. N. (2022). Hydrochemistry of medium-size pristine rivers in boreal and subarctic zone: Disentangling effect of landscape parameters across a permafrost, climate, and vegetation gradient. *Water*, *14*(14), 2250. https://doi.org/10.3390/w14142250

Pokrovsky, O. S., Manasypov, R. M., Chupakov, A. V., & Kopysov, S. (2022). Element transport in the Taz River, western Siberia. *Chemical Geology*, *614*, 121180. https://doi.org/10.1016/j.chemgeo.2022.121180

Pokrovsky, O. S., Manasypov, R. M., Kopysov, S. G., Krickov, I. V., Shirokova, L. S., Loiko, S. V., et al. (2020). Impact of permafrost thaw and climate warming on riverine export fluxes of carbon, nutrients and metals in Western Siberia. *Water*, *12*(6), 1817. https://doi.org/10.3390/w12061817

Pokrovsky, O. S., Manasypov, R. M., Loiko, S., Shirokova, L. S., Krickov, I. A., Pokrovsky, B. G., et al. (2015). Permafrost coverage, watershed area and season control of dissolved carbon and major elements in western Siberian rivers. *Biogeosciences*, *12*(21), 6301–6320. https://doi.org/10.5194/bg-12-6301-2015

Pokrovsky, O. S., Manasypov, R. M., Loiko, S. V., Krickov, I. A., Kopysov, S. G., Kolesnichenko, L. G., et al. (2016). Trace element transport in western Siberian rivers across a permafrost gradient. *Biogeosciences*, *13*(6), 1877–1900. https://doi.org/10.5194/bg-13-1877-2016

Poulin, B. A., Ryan, J. N., Nagy, K. L., Stubbins, A., Dittmar, T., Orem, W., et al. (2017). Spatial dependence of reduced sulfur in everglades dissolved organic matter controlled by sulfate enrichment. *Environmental Science & Technology*, *51*(7), 3630–3639. https://doi.org/10.1021/acs.est.6b04142

Raeke, J., Lechtenfeld, O. J., Wagner, M., Herzsprung, P., & Reemtsma, T. (2016). Selectivity of solid phase extraction of freshwater dissolved organic matter and its effect on ultrahigh resolution mass spectra. *Environmental Science: Processes & Impacts*, *18*(7), 918–927. https://doi.org/10.1039/C6EM00200E

Rantala, M. V., Nevalainen, L., Rautio, M., Galkin, A., & Luoto, T. P. (2016). Sources and controls of organic carbon in lakes across the subarctic treeline. *Biogeochemistry*, *129*(1–2), 235–253. https://doi.org/10.1007/s10533-016-0229-1

Raudina, T. V., Smirnov, S. V., Lushchaeva, I. V., Istigechev, G. I., Kulizhskiy, S. P., Golovatskaya, E. A., et al. (2022). Seasonal and spatial variations of dissolved organic matter biodegradation along the aquatic continuum in the Southern Taiga bog complex, Western Siberia. *Water*, *14*(23), 3969. https://doi.org/10.3390/w14233969

Raymond, P. A., McClelland, J. W., Holmes, R. M., Zhulidov, A. V., Mull, K., Peterson, B. J., et al. (2007). Flux and age of dissolved organic carbon exported to the Arctic Ocean: A carbon isotopic study of the five largest arctic rivers. *Global Biogeochemical Cycles*, *21*(4), 2007GB002934. https://doi.org/10.1029/2007GB002934

R Core Team. (2020). R: A language and environment for statistical computing, *The R Project for Statistical Computing*. Retrieved from https://www.r-project.org/

Revelle, W. (2024). psych: Procedures for Psychological, Psychometric, and Personality Research (Version 2.4.6.26) [Computer software]. *CRAN*. https://cran.r-project.org/web/packages/psych/index.html

Rodríguez-Cardona, B. M., Coble, A. A., Wymore, A. S., Kolosov, R., Podgorski, D. C., Zito, P., et al. (2020). Wildfires lead to decreased carbon and increased nitrogen concentrations in upland arctic streams. *Scientific Reports*, *10*(1), 8722. https://doi.org/10.1038/s41598-020-65520-0

Rogers, J. A., Galy, V., Kellerman, A. M., Chanton, J. P., Zimov, N., & Spencer, R. G. M. (2021). Limited presence of permafrost dissolved organic matter in the Kolyma River, Siberia revealed by ramped oxidation. *Journal of Geophysical Research: Biogeosciences*, *126*(7), e2020JG005977. https://doi.org/10.1029/2020JG005977

Romanovsky, V. E., Drozdov, D. S., Oberman, N. G., Malkova, G. V., Kholodov, A. L., Marchenko, S. S., et al. (2010). Thermal state of permafrost in Russia. *Permafrost and Periglacial Processes*, *21*(2), 136–155. https://doi.org/10.1002/ppp.683

Rosset, T., Binet, S., Rigal, F., & Gandois, L. (2022). Peatland dissolved organic carbon export to surface waters: Global significance and effects of anthropogenic disturbance. *Geophysical Research Letters*, *49*(5), e2021GL096616. https://doi.org/10.1029/2021GL096616

Sada, R., Schmalz, B., Kiesel, J., & Fohrer, N. (2019). Projected changes in climate and hydrological regimes of the Western Siberian lowlands. *Environmental Earth Sciences*, *78*(2), 56. https://doi.org/10.1007/s12665-019-8047-0

Šantl-Temkiv, T., Finster, K., Dittmar, T., Hansen, B. M., Thyrhaug, R., Nielsen, N. W., & Karlson, U. G. (2013). Hailstones: A window into the microbial and chemical inventory of a storm cloud. *PLoS One*, *8*(1), e53550. https://doi.org/10.1371/journal.pone.0053550

Savory, J. J., Kaiser, N. K., McKenna, A. M., Xian, F., Blakney, G. T., Rodgers, R. P., et al. (2011). Parts-per-billion Fourier transform ion cyclotron resonance mass measurement accuracy with a "walking" calibration equation. *Analytical Chemistry*, *83*(5), 1732–1736. https://doi.org/10.1021/ac102943z

Schuur, E. A. G., Abbott, B. W., Commane, R., Ernakovich, J., Euskirchen, E., Hugelius, G., et al. (2022). Permafrost and climate change: Carbon cycle feedbacks from the warming Arctic. *Annual Review of Environment and Resources*, *47*(1), 343–371. https://doi.org/10.1146/annurev-environ-012220-011847

Schuur, E. A. G., McGuire, A. D., Schädel, C., Grosse, G., Harden, J. W., Hayes, D. J., et al. (2015). Climate change and the permafrost carbon feedback. *Nature*, *520*(7546), 171–179. https://doi.org/10.1038/nature14338

Serikova, S., Pokrovsky, O. S., Ala-Aho, P., Kazantsev, V., Kirpotin, S. N., Kopysov, S. G., et al. (2018). High riverine CO_2 emissions at the permafrost boundary of Western Siberia. *Nature Geoscience*, *11*(11), 825–829. https://doi.org/10.1038/s41561-018-0218-1

Serikova, S., Pokrovsky, O. S., Laudon, H., Krickov, I. V., Lim, A. G., Manasypov, R. M., & Karlsson, J. (2019). High carbon emissions from thermokarst lakes of Western Siberia. *Nature Communications*, *10*(1), 1552. https://doi.org/10.1038/s41467-019-09592-1

Sheng, Y., Smith, L. C., MacDonald, G. M., Kremenetski, K. V., Frey, K. E., Velichko, A. A., et al. (2004). A high-resolution GIS-based inventory of the west Siberian peat carbon pool. *Global Biogeochemical Cycles*, *18*(3). https://doi.org/10.1029/2003GB002190

Smith, D. F., Podgorski, D. C., Rodgers, R. P., Blakney, G. T., & Hendrickson, C. L. (2018). 21 Tesla FT-ICR mass spectrometer for ultrahigh-resolution analysis of complex organic mixtures. *Analytical Chemistry*, *90*(3), 2041–2047. https://doi.org/10.1021/acs.analchem.7b04159

Spencer, R. G. M., Aiken, G. R., Butler, K. D., Dornblaser, M. M., Striegl, R. G., & Hernes, P. J. (2009). Utilizing chromophoric dissolved organic matter measurements to derive export and reactivity of dissolved organic carbon exported to the Arctic Ocean: A case study of the Yukon River, Alaska. *Geophysical Research Letters*, *36*(6), 2008GL036831. https://doi.org/10.1029/2008GL036831

Spencer, R. G. M., Butler, K. D., & Aiken, G. R. (2012). Dissolved organic carbon and chromophoric dissolved organic matter properties of rivers in the USA. *Journal of Geophysical Research*, *117*(G3), 2011JG001928. https://doi.org/10.1029/2011JG001928

Spencer, R. G. M., Kellerman, A. M., Podgorski, D. C., Macedo, M. N., Jankowski, K., Nunes, D., & Neill, C. (2019). Identifying the molecular signatures of agricultural expansion in Amazonian headwater streams. *Journal of Geophysical Research: Biogeosciences*, *124*(6), 1637–1650. https://doi.org/10.1029/2018JG004910

Spencer, R. G. M., Mann, P. J., Dittmar, T., Eglinton, T. I., McIntyre, C., Holmes, R. M., et al. (2015). Detecting the signature of permafrost thaw in Arctic rivers. *Geophysical Research Letters*, *42*(8), 2830–2835. https://doi.org/10.1002/2015GL063498

Starr, S., Johnston, S. E., Sobolev, N., Perminova, I., Kellerman, A., Fiske, G., et al. (2023). Characterizing uncertainty in Pan-Arctic land-ocean dissolved organic carbon flux: Insights from the Onega River, Russia. *Journal of Geophysical Research: Biogeosciences*, *128*(5), e2022JG007073. https://doi.org/10.1029/2022JG007073

Starr, S. F., Frey, K. E., Smith, L. C., Kellerman, A. M., McKenna, A. M., & Spencer, R. G. M. (2024). Peatlands versus permafrost: Landscape features as drivers of dissolved organic matter composition in West Siberian rivers. *Journal of Geophysical Research: Biogeosciences*, *129*(2), e2023JG007797. https://doi.org/10.1029/2023JG007797

Tarnocai, C., Canadell, J. G., Schuur, E. A. G., Kuhry, P., Mazhitova, G., & Zimov, S. (2009). Soil organic carbon pools in the northern circumpolar permafrost region. *Global Biogeochemical Cycles*, *23*(2), GB2023. https://doi.org/10.1029/2008GB003327

Textor, S. R., Wickland, K. P., Podgorski, D. C., Johnston, S. E., & Spencer, R. G. M. (2019). Dissolved organic carbon turnover in permafrost-influenced watersheds of interior Alaska: Molecular insights and the priming effect. *Frontiers in Earth Science*, *7*, 275. https://doi.org/10.3389/feart.2019.00275

Tranvik, L. J., Downing, J. A., Cotner, J. B., Loiselle, S. A., Striegl, R. G., Ballatore, T. J., et al. (2009). Lakes and reservoirs as regulators of carbon cycling and climate. *Limnology and Oceanography*, *54*(6part2), 2298–2314. https://doi.org/10.4319/lo.2009.54.6_part_2.2298

Valle, J., Gonsior, M., Harir, M., Enrich-Prast, A., Schmitt-Kopplin, P., Bastviken, D., et al. (2018). Extensive processing of sediment pore water dissolved organic matter during anoxic incubation as observed by high-field mass spectrometry (FTICR-MS). *Water Research*, *129*, 252–263. https://doi.org/10.1016/j.watres.2017.11.015

Vorobyev, S. N., Pokrovsky, O. S., Kirpotin, S. N., Kolesnichenko, L. G., Shirokova, L. S., & Manasypov, R. M. (2015). Flood zone biogeochemistry of the Ob River middle course. *Applied Geochemistry*, *63*, 133–145. https://doi.org/10.1016/j.apgeochem.2015.08.005

Vorobyev, S. N., Pokrovsky, O. S., Kolesnichenko, L. G., Manasypov, R. M., Shirokova, L. S., Karlsson, J., & Kirpotin, S. N. (2019). Biogeochemistry of dissolved carbon, major, and trace elements during spring flood periods on the Ob River. *Hydrological Processes*, *33*(11), 1579–1594. https://doi.org/10.1002/hyp.13424

Vorobyev, S. N., Pokrovsky, O. S., Korets, M., & Shirokova, L. S. (2022). A snap-shot assessment of carbon emission and export in a pristine river draining permafrost peatlands (Taz River, Western Siberia). *Frontiers in Environmental Science*, *10*, 987596. https://doi.org/10.3389/fenvs.2022.987596

Weishaar, J. L., Aiken, G. R., Bergamaschi, B. A., Fram, M. S., Fujii, R., & Mopper, K. (2003). Evaluation of specific ultraviolet absorbance as an indicator of the chemical composition and reactivity of dissolved organic carbon. *Environmental Science & Technology*, *37*(20), 4702–4708. https://doi.org/10.1021/es030360x

Wickham, H. (2016). *ggplot2: Elegant Graphics for Data Analysis* (2nd ed.). Springer International Publishing. https://doi.org/10.1007/978-3-319-24277-4

Wilson, H. F., & Xenopoulos, M. A. (2009). Effects of agricultural land use on the composition of fluvial dissolved organic matter. *Nature Geoscience*, *2*(1), 37–41. https://doi.org/10.1038/ngeo391

Xian, F., Hendrickson, C. L., Blakney, G. T., Beu, S. C., & Marshall, A. G. (2010). Automated broadband phase correction of Fourier transform ion cyclotron resonance mass spectra. *Analytical Chemistry*, *82*(21), 8807–8812. https://doi.org/10.1021/ac101091w

Xu, M., Kang, S., Wang, X., Wu, H., Hu, D., & Yang, D. (2020). Climate and hydrological changes in the Ob River Basin during 1936–2017. *Hydrological Processes*, *34*(8), 1821–1836. https://doi.org/10.1002/hyp.13695

Yeghicheyan, D., Aubert, D., Coz, M. B., Chmeleff, J., Delpoux, S., Djouraev, I., et al. (2019). A new interlaboratory characterisation of silicon, rare Earth elements and twenty-two other trace element concentrations in the natural river water certified reference material SLRS-6 (NRC-CNRC). *Geostandards and Geoanalytical Research*, *43*(3), 475–496. https://doi.org/10.1111/ggr.12268

Yvin, O. M., Kurek, M. R., McKenna, A. M., Hawkings, J. R., & Spencer, R. G. M. (2024). Comparison of dissolved organic matter composition from various sorbents using ultra-high resolution mass spectrometry. *Organic Geochemistry*, *196*, 104846. https://doi.org/10.1016/j.orggeochem.2024.104846

References From the Supporting Information

Blakney, G. T., Hendrickson, C. L., & Marshall, A. G. (2011). Predator data station: A fast data acquisition system for advanced FT-ICR MS experiments. *International Journal of Mass Spectrometry*, *306*(2), 246–252. https://doi.org/10.1016/j.ijms.2011.03.009

Boldin, I. A., & Nikolaev, E. N. (2011). Fourier transform ion cyclotron resonance cell with dynamic harmonization of the electric field in the whole volume by shaping of the excitation and detection electrode assembly. *Rapid Communications in Mass Spectrometry*, *25*(1), 122–126. https://doi.org/10.1002/rcm.4838

Chen, T., Beu, S. C., Kaiser, N. K., & Hendrickson, C. L. (2014). Note: Optimized circuit for excitation and detection with one pair of electrodes for improved Fourier transform ion cyclotron resonance mass spectrometry. *Review of Scientific Instruments*, *85*(6), 066107. https://doi.org/10.1063/1.4883179

Harris, I., Jones, P., Osborn, T., & Lister, D. (2014). Updated high-resolution grids of monthly climatic observations—The CRU TS3.10 Dataset. *International Journal of Climatology*, *34*(3), 623–642. https://doi.org/10.1002/joc.3711

Hugelius, G., Bockheim, J. G., Camill, P., Elberling, B., Grosse, G., Harden, J. W., et al. (2013). A new data set for estimating organic carbon storage to 3 m depth in soils of the northern circumpolar permafrost region. *Earth System Science Data*, *5*(2), 393–402. https://doi.org/10.5194/essd-5-393-2013

Hughey, C. A., Hendrickson, C. L., Rodgers, R. P., Marshall, A. G., & Qian, K. (2001). Kendrick mass defect spectrum: A compact visual analysis for ultrahigh-resolution broadband mass spectra. *Analytical Chemistry*, *73*(19), 4676–4681. https://doi.org/10.1021/ac010560w

Kaiser, N. K., McKenna, A. M., Savory, J. J., Hendrickson, C. L., & Marshall, A. G. (2013). Tailored ion radius distribution for increased dynamic range in FT-ICR mass analysis of complex mixtures. *Analytical Chemistry*, *85*(1), 265–272. https://doi.org/10.1021/ac302678v

Kendrick, E. (1963). A mass scale based on $CH_2 = 14.0000$ for high resolution mass spectrometry of organic compounds. *Analytical Chemistry*, *35*(13), 2146–2154. https://doi.org/10.1021/ac60206a048